Extended aerosol and surface characterization from S5P/TROPOMI with GRASP algorithm. Part I: Conditions, approaches, performance and new possibilities

Pavel Litvinov, Cheng Chen, Oleg Dubovik, Lukas Bindreiter, Christian Matar, David Fuertes, Anton Lopatin, Tatyana Lapyonok, Verena Lanzinger, Andreas Hangler, et al.

Remote Sensing of Environment 313 (2024) 114355

Contents lists available at ScienceDirect

Remote Sensing of Environment

journal homepage: www.elsevier.com/locate/rse

Extended aerosol and surface characterization from S5P/TROPOMI with GRASP algorithm. Part I: Conditions, approaches, performance and new possibilities

Pavel Litvinov [a,*], Cheng Chen [a,g,*], Oleg Dubovik [b], Lukas Bindreiter [c], Christian Matar [a], David Fuertes [a], Anton Lopatin [a], Tatyana Lapyonok [b], Verena Lanzinger [c], Andreas Hangler [c], Michael Aspetsberger [c], Martin de Graaf [d], Lieuwe Gijsbert Tilstra [d], Piet Stammes [d], Alexandru Dandocsi [e], Daniele Gasbarra [f], Elody Fluck [e], Claus Zehner [e], Christian Retscher [e]

[a] GRASP SAS, Remote Sensing Developments, 3 rue Louis Néel, 59260 Lezennes, France
[b] Univ. Lille, CNRS, UMR–8518 – LOA - Laboratoire d'Optique Atmosphérique, F-59000, France
[c] Cloudflight, 23 Huemerstrasse, Linz, Austria
[d] KNMI, De Bilt, 297 Utrechtseweg, the Netherlands
[e] ESA-ESRIN, 1 Via Galilei, Frascati 00044, Italy
[f] Shamrock Space Services, c/o ESA-ESRIN, 1 Via Galilei, Frascati 00044, Italy
[g] Anhui Institute of Optics and Fine Mechanics, Hefei Institutes of Physical Science, Chinese Academy of Sciences, Hefei 230031, China

ARTICLE INFO

Keywords:
Aerosol and surface remote sensing
Aerosol retrieval algorithm
Surface BRDF and aerosol models
Aerosol extended properties
S5p/TROPOMI measurements

ABSTRACT

Atmospheric aerosols have strong impact on climate, environment, and health. To account correctly for such impact, extended aerosol characterization, including spectral Aerosol Optical Depth (AOD), Angstrom Exponent (AE), spectral Single Scattering Albedo (SSA) etc., are required to be derived globally from space-borne observations. Together with the aerosol, the Earth's surfaces are an important component of climate system, reflecting and absorbing solar and atmospheric radiation and being sources of emission of different natural aerosol, for example, sea-salt, mineral dust or organic aerosol.

Since the beginning of space-borne atmospheric observation it was recognized that the most comprehensive extended aerosol and surface characterization can be achieved from multi-angular polarimetric measurements. In this paper, we show that the extended aerosol characterization can be obtained even from single viewing radiance only satellite measurements when several crucial conditions are fulfilled both for the observations and retrieval algorithm: (i) wide spectral range (for example, covering UV, VIR, NIR and SWIR spectra) providing rich spectral information about aerosol and surface; (ii) wide swath of measurements ensuring frequent overpassing over the same ground pixel to account for the different temporal variability of aerosol and surface properties as well as for angular dependence of surface reflectance; (iii) applied algorithm should be able to treat multi-temporal and multi-spatial observation accounting for spatial and temporal dependencies of aerosol and surface characteristics.

The new possibilities of retrieval of aerosol and surface properties are investigated by applying the advanced GRASP (Generalized Retrieval of Atmosphere and Surface Properties) algorithm to the space-borne S5P/TROPOMI observations. The most optimal for these purposes forward and inversion approaches are discussed, and the quality of retrieved aerosol and surface properties is evaluated. The possibilities of TROPOMI/GRASP approach for aerosol extended characterization are demonstrated on several aerosol events including dust storms, biomass burning and anthropogenic aerosol pollution outbreaks in worldwide locations.

Editor: Menghua Wang

* Corresponding authors at: GRASP SAS, Remote Sensing Developments, 3 rue Louis Néel, 59260 Lezennes, France.
E-mail addresses: Pavel.Litvinov@grasp-sas.com (P. Litvinov), Cheng.Chen@grasp-sas.com (C. Chen).

https://doi.org/10.1016/j.rse.2024.114355
Received 22 December 2023; Received in revised form 18 June 2024; Accepted 3 August 2024
Available online 16 August 2024

1. Introduction

The global information about aerosol becomes increasingly important for different atmospheric applications due its big effect on climate and environment. The estimation of this effect is associated with well-known high uncertainties in the global aerosol characterization (IPCC, 2021). The air quality assessment and emission estimates rely more and more on accurate and global aerosol data (Dubovik et al., 2008; Martin, 2008; Chen et al., 2019, 2022a). Moreover, the global information about aerosol is crucial for such applications as atmospheric trace gases characterization and atmospheric correction for land and ocean studies (Veefkind et al., 2012; Lyapustin et al., 2011, 2018; Vermote and Kotchenova, 2008).

Together with the atmospheric aerosol, the Earth's surfaces play a crucial role in the climate system through radiative interaction with atmosphere and being natural sources of primary emission of different aerosol species (for example, sea-salt, mineral dust, organic aerosol etc.). The surface reflection properties strongly affect the Earth's energetic balance and should be accurately accounted for in global climate studies.

The retrieval of aerosol and surface properties from remote sensing measurements are closely related to each other. In particular, a correct surface reflection description is absolutely required for an accurate characterization of such atmospheric components as aerosol, cloud and trace gases. At the same time, an accurate characterization of surface reflectance is not possible without knowledge about atmosphere properties.

The most comprehensive information about aerosol scattering and absorption properties is contained in multi-angular, multi-spectral, photopolarimetric measurements (Van de Hulst, 1957; Bohren and Huffman, 1998; Mishchenko et al., 2002). Therefore, since the beginning of the atmospheric remote sensing studies, the instruments with such measurement possibilities were considered as the most suitable for full microphysical properties retrieval of aerosol (Travis, 1992, 1993; Deschamps et al., 1994; Mishchenko and Travis, 1997; Mishchenko et al., 2004). Moreover, such observations essentially improve the separation of atmosphere and surface signals which results in more advanced aerosol characterization (Herman et al., 1999; Hasekamp and Landgraf, 2007; Hasekamp et al., 2011, 2024; Dubovik et al., 2011, 2021a; Chen et al., 2020). At present, an essential number of satellites have been launched to support different climate studies (Deschamps et al., 1994; Remer et al., 2005; Tanré et al., 2011; Hollmann et al., 2013; de Araujo Barbosa et al., 2015; Cao et al., 2013; Dubovik et al., 2019). Despite the known advantage of multi-viewing polarimetric measurements, POLDER-1, 2 and 3 instruments were the only space-borne polarimeters operating for quite long period 1996, 2002 and from 2005 to 2013 years. Single-viewing observations are currently still the main global and long-term sources of information about aerosol and surface. Aerosol Optical Depth (AOD), representing the amount of aerosol in the atmospheric column, is the main aerosol product derived from the most satellite missions (Levy et al., 2013; de Leeuw et al., 2015; Popp et al., 2016; Torres et al., 2007, 2013; Sayer et al., 2018a; Sayer et al., 2018b). The accuracy of extended aerosol characterization from space-borne remote sensing, including particle size and absorption properties, still requires essential improvements (Li et al., 2009; Kokhanovsky, 2013; Dubovik et al., 2019, 2021a, 2021b; Chen et al., 2020; Schutgens et al., 2021).

The quality of extended aerosol and surface characterization from single viewing instruments can be considerably enhanced with advanced retrieval approaches. One of the possibilities is to consider temporal and spatial dependences between the characteristics of aerosol or surface, which are not accounted for in traditional retrieval algorithms. Indeed, the properties of aerosol do not change randomly in time and space but rather are related to each other by atmospheric dynamic processes. Surface properties can be very inhomogeneous in space, but, usually, show strong temporal correlations. Full physical consideration of the spatial and temporal dependencies of atmosphere or surface properties in the retrieval algorithms has not been implemented yet. Nevertheless, such correlations can be accounted for by the retrieval constraints, allowing accumulating multi-angular, temporal and spatial information about atmosphere and surface. This approach was realized in the GRASP (Generalized Retrieval of Atmosphere and Surface Properties) algorithm as a multi-pixel retrieval, when large groups of pixels within several satellite overpasses are retrieved simultaneously with applied spatial and temporal smoothness constraints on the variability of aerosol and surface parameters (Dubovik et al., 2011, 2014, 2021b).

The GRASP algorithm is very generalized and designed to be applicable to different observations. Nevertheless, its adaptation to specific instrument as well as retrieval quality depends strongly on the information content of the measurements and requires separate studies on the most optimal forward models, observation data preparation and different kind of physical and algorithmic constraints.

Enhanced performance in aerosol characterization with GRASP algorithm was demonstrated on PARASOL/POLDER observations (Chen et al., 2020; Schutgens et al., 2021). Application of the GRASP to Sentinel-3/OLCI instrument also showed a performance comparable to MODIS AOD retrievals. At the same time, the studies showed the dependence of the quality of AOD OLCI/GRASP retrieval on a priori information about surface BRDF (Bi-Directional Reflectance Distribution Function) and reduced quality of retrieval of the extended properties like Angstrom Exponent (AE) and Single Scattering Albedo (SSA) (Chen et al., 2022b).

In this paper, applying GRASP algorithm to S5P/TROPOMI observations, we explore the possibilities and conditions to derive advanced aerosol and surface products from single viewing space-borne measurements. The Copernicus S5P/TROPOMI instrument, launched on 13 October 2017, takes a special place among all currently operating satellites (Veefkind et al., 2012). It provides hyperspectral measurements in a wide spectral range covering ultraviolet (UV), visible (VIS), near-infrared (NIR) and shortwave infrared (SWIR) containing essential pieces of information required for advanced aerosol and surface characterization. At present, the high potential of TROPOMI capabilities has not been fully explored for detailed characterization of aerosol and surface properties.

This paper is the first one of two companioning articles describing the TROPOMI/GRASP studies, developments and derived extended product of aerosol and surface properties. The special attention is paid to the physical description and justification of the forward modelling and inversion approaches required for extended aerosol and surface characterization from single-viewing observations. To understand the advantages and limitations of the main assumptions of the applied methods, the validation criteria are formulated in the paper. They are used to evaluate the quality of the TROPOMI/GRASP extended products against AERONET and other reference datasets. The possibilities of advanced extended aerosol characterization with GRASP algorithm applied to S5P/TROPOMI measurements are demonstrated on several known aerosol events including Biomass Burning (BB) outbreaks, anthropogenic pollution, and Dust storms in worldwide locations. Analyzing TROPOMI/GRASP approaches and product validation results, the conditions for extended aerosol and surface characterization from single-viewing observations are discussed and formulated in this paper. The Part II companion article will be focused on the extensive intercomparison of globally retrieved TROPOMI/GRASP parameters with other products such as VIIRS and MODIS aerosol and surface products (Chen et al., 2024).

2. S5P/TROPOMI data for GRASP retrieval

The GRASP algorithm is designed with the idea of taking advantage from the full available spectral and angular information of observations (Dubovik et al., 2011, 2014, 2021b). To achieve the best retrieval quality all measurements should be prepared in a uniform way for all

spectral channels and the observations over different pixels should be united in spatial and temporal blocks for simultaneous inversion.

Since the main objective of S5P/TROPOMI mission is to monitor trace gases relevant for air quality and climate, the instrument was designed for collecting hyperspectral radiances from UV to SWIR spectral range. However, because the scattering and absorption of aerosols are spectrally quite smooth, GRASP aerosol retrieval from TROPOMI was set up for inverting only at 10 spectral bands of 1 nm width selected outside of strong gas absorption lines (in the continuum parts of the spectrum) in the range 340–2314 nm (Table 1). The averaging over all measurements in the 1 nm bandwidth was performed using a triangular weight function with a value equal to 1 at the selected central band position and 0 at the edges (TROPOMI ATBD of the KNMI AOT, 2022). Such a triangular weighting function avoids jumps in the averaged reflectances along the across-track direction of the orbit swath at the band edges, where detector pixels are irregularly part of the averaging procedure. The positions of the selected 10 bands take into account the nonlinearity of the surface reflectance spectral dependence on different surface types. They are proposed as a reference bands for interpolation and extrapolation into other wavelengths to support a number of current and future S5P/TROPOMI atmospheric products relying on the surface reflection information. As it will be discussed in the next sections, the range from UV to SWIR allows enhancing retrieval sensitivity to aerosol size, absorption and scattering properties, as well as better differentiating between aerosol and surface signals.

The S5P/TROPOMI spatial resolution is different for different spectral ranges (TROPOMI L1B Specification, 2022). For example, the TROPOMI UV-VIS-NIR detector (bands 3, 4, 5, 6) has spatial resolution 5.5 km (along-track) x 3.5 km (across-track) at nadir, and the SWIR (band 7) has 5.5 km (along-track) x 7 km (across-track). Since GRASP/TROPOMI retrieval was performed simultaneously at all selected spectral bands, the TROPOMI radiances for all channels were regridded under equidistant cylindrical projection and WGS84 coordinate system to the same spatial pixel resolution of 0.09°, which is close to the resolution in SWIR range. The bilinear regridding method was used for this purpose (https://gdal.org/programs/gdalwarp.html).

As it will be described below, in order to achieve the best quality of aerosol and surface retrieval TROPOMI/GRASP processing over sea/ocean the auxiliary information about wind speed at surface boundary level was used (Table 1). The values of wind speed were adopted from collocated S5P Level 2 Nitrogen Dioxide (NO2) product.

(https://sentinels.copernicus.eu/web/sentinel/data-products/-/asset_publisher/fp37fc19FN8F/content/sentinel-5-precursor-level-2-nitrogen-dioxide) where the eastward and northward horizontal components of 10 m height wind is originally obtained from ECMWF data.

The calibration accuracy of the TROPOMI radiance data is important for the GRASP retrievals. The in-flight calibration of the instrument has been described by Ludewig et al. (2020), whereas the first validation of the TROPOMI L1B radiances has been performed by Tilstra et al. (2020). It appears that the calibration depends on the wavelength and lies between 0 and 7% for the selected channels.

TROPOMI predecessors, OMI and SCIAMACHY, were suffering from cloud contamination due to rather coarse spatial resolution (Bovensmann et al., 1999; Burrows et al., 1995; Levelt et al., 2006; Veefkind et al., 2012). The cloud screening in TROPOMI/GRASP processing is based on the S5P NPP-VIIRS cloud product with about 500 m spatial resolution. The orbits of S5P/TROPOMI and NPP-VIIRS are similar with current time difference approximately 3 min. The cloud information from VIIRS is provided for each individual TROPOMI regridded pixel and for spectral bands 380, 494, and 670 nm (3, 6 and 7 in Table 1). For TROPOMI/GRASP retrieval the pixels are considered as cloud free if the cloud fraction for all spectral bands 3, 6, and 7 is equal or <10%.

3. Baseline requirements on aerosol and surface properties

Different applications impose different requirements on aerosol and surface dataset. Most comprehensive and detailed requirements on aerosol characterization from space-borne missions were formulated by the climate organizations and groups Global Climate Observing System (GCOS, 2016), Climate Modelling User Group (CMUG, 2015), ESA aerosol Climate Change Initative (CCI, 2019) and published in a number of scientific papers and reports (Kinne et al., 2006; Popp et al., 2016).

The summary of these GCOS-based requirements for such aerosol characteristics as AOD, AODF (fine mode AOD), SSA (single scattering albedo) and AE (Angstrom Exponent) are presented in the Table 2 as “Optimal”. The fulfilment of “optimal” (or GCOS-based) requirements may be challenging for space-borne remote sensing retrieval and too strict for a number of applications where correction for aerosol does not require such accuracy. At present, no existing aerosol data product can meet them completely especially for such extended aerosol properties as SSA, AE etc. (Popp et al., 2016; Chen et al., 2020; Dubovik et al., 2021b). Therefore, to demonstrate the retrieval performance at different conditions relaxed but still quite demanding “Target” requirements on aerosol optical characteristics were defined in the frame of S5P + I AOD/BRDF project and summarized in Table 2 (TROPOMI, 2022b). Both “Optimal” and “Target” requirements were formulated for the aerosol optical properties since they can be validated much more reliably than microphysical ones (e.g., complex refractive index, size distribution parameters, non-sphericity, etc.) validation for which is much more complicated due to luck of direct reliable observations of these parameters.

The requirements for such surface characteristics as the surface reflectance and different kinds of surface albedos have been formulated by GCOS and extended for surface characterization from space-borne measurements, for example, from Sentinel-3, − 4, S5P/TROPOMI etc.

Table 2
Requirements on aerosol and surface characteristics.

Characteristics	Required uncertainty	
	Optimal	Target
AOD	0.04 or 10% (whatever is bigger)	0.05 or 20% (whatever is bigger)
fine mode AOD (AODF)	0.04 or 10% (whatever is bigger)	0.05 or 20% (whatever is bigger)
SSA	0.03	0.05
AE (443–670)	0.3	0.5
First BRDF parameter, Surface reflectance, Albedos	0.01	0.02

Table 1
S5P/TROPOMI measurements and auxiliary input for GRASP processing.

Central band position, nm	340	367	380	416	440	494	670	740	772	2313
Band ID	3			4			5	6		7
L1B Spatial Sampling	5.5 km × 3.5 km									5.5 km × 7 km
Spectral resolution	1 nm									
Spatial resolution	0.09 degree (equidistant cylindrical projection and WGS84)									
Auxiliary Information	Wind speed information (ECMWF)									
Cloud masking	S5P NPP-VIIRS Cloud Mask									

(GCOS, 2016; TROPOMI, 2022b). The compilation of such requirements used for TROPOMI/GRASP studies is provided in the Table 2 in terms of "optimal" and "target" absolute uncertainties of surface characteristics, demonstrating the dynamic performance of surface products.

4. GRASP algorithm forward modelling and numerical inversion approaches for S5P/TROPOMI measurements

4.1. GRASP forward model approaches for S5P/TROPOMI retrieval

4.1.1. Aerosol model

GRASP approaches for modelling aerosol optical properties are very flexible and can be chosen depending on the information content of the measurements: it may be based on "full microphysical" aerosol characterization or simplified but still efficient "aerosol models" approach (Dubovik and King, 2000; Dubovik et al., 2011, 2021b; Chen et al., 2020, 2022b; Lopatin et al., 2021).

GRASP "full microphysical approach with 5 lognormal bins for the Size Distribution description was successfully used for processing data of the POLDER-1, −2 and POLDER-3/PARASOL instruments providing multi-angular polarimetric measurements in VIS and NIR spectral ranges (Dubovik et al., 2011, 2021b; Chen et al., 2020).

The rather simplified GRASP "models" approach was demonstrated to be efficient for data interpretation both from the instruments with extensive multi-angular and polarimetric capabilities (POLDER-1, −2 and POLDER-3/PARASOL instruments) and from the instruments with limited information content (Envisat/MERIS, Sentinel-3/OLCI) (Chen et al., 2020; Lopatin et al., 2021; Dubovik et al., 2021b; Chen et al., 2022b).

Both aerosol "full microphysical" and "models" approaches were extensively tested on S5P/TROPOMI measurements. The retrievals of aerosol properties using both approaches with adequate constraints on the aerosol parameters showed good performance, based on the comparisons with AERONET. GRASP "models" approach demonstrated slightly better performance in terms of the required processing time and stability in possible presence of cloud contamination or gaps in the observations due to cloudy conditions. Therefore, this approach was selected as a baseline for global processing of S5P/TROPOMI observations (TROPOMI ATBD of GRASP AOD + BRDF, 2022).

The total single scattering characteristics of aerosol in the "models" approach are represented as the linear combinations of the scattering characteristics of the preselected aerosol components i.e. assuming external mixture of different aerosol models. Namely, the total aerosol extinction and scattering optical depths (τ_{ext}^{aer}, τ_{sc}^{aer}), phase matrix ($\mathbf{P}^{aer}$) and single scattering albedo (SSA, ω^{aer}) can be obtained as following:

$$\tau_{ext}^{aer}(\lambda) = c_v^{(o)} \sum_{k=1}^{n_k} c_k C_{ext}^k(\lambda) \tag{1a}$$

$$\tau_{sc}^{aer}(\lambda) = c_v^{(0)} \sum_{k=1}^{n_k} c_k C_{sc}^k(\lambda), \quad \omega^{aer}(\lambda) = \frac{\tau_{sc}^{aer}(\lambda)}{\tau_{ext}^{aer}(\lambda)} \tag{1b}$$

$$\omega^{aer}(\lambda)\mathbf{P}^{aer}(\lambda,\vartheta) = \frac{\sum_{k=1}^{n_k} c_k C_{ext}^k(\lambda)\omega_k \mathbf{P}_k(\lambda,\vartheta)}{\sum_{k=1}^{n_k} c_k C_{ext}^k(\lambda),} \tag{1c}$$

In Eqs. (1a)-(1c) index k denotes certain aerosol component in GRASP "models" approach. Four different aerosol components were used to process S5P/TROPOMI measurements ($n_k = 4$): 1) the fine absorbing one ($k = 1$) representing climatological biomass burning aerosol model; 2) the fine slightly absorbing ($k = 2$) model corresponding to climatological sulphate aerosols with introduced minor absorption; 3) the coarse component representing mainly maritime aerosol type ($k = 3$) and 4) the coarse component for dust aerosol representation ($k = 4$). $C_{ext}^k(\lambda)$ and $C_{sc}^k(\lambda)$ in Eqs. (1)–(3) are the extinction and scattering cross sections per unit particle volume (with dimension $\left[C_{ext/sc}^k\right] = \mu m^{-1}$) for each aerosol component and $\mathbf{P}_k(\lambda,\vartheta)$ is their phase matrix. In GRASP "models" approach both cross sections $C_{ext/sc}^k(\lambda)$ and phase matrices $\mathbf{P}_k(\lambda,\vartheta)$ of aerosol are precalculated for each selected S5P/TROPOMI spectral band (at central wavelength λ, see Table 1) with size distribution parameters, spectral complex refractive indices, and non-sphericity parameters corresponding to each aerosol component k (Lopatin et al., 2021). Therefore, only five spectrally independent aerosol parameters are retrieved by GRASP from S5P/TROPOMI measurements: the total column volume concentration $c_v^{(0)}$ ($\left[c_v^{(0)}\right] = \mu m$) and four relative fractions for each aerosol component c_k ($\sum_k c_k = 1$) (Eqs. (1)–(3)). These retrieved parameters allow calculating the total optical properties of atmospheric aerosol at any spectral band using precalculated cross sections and phase matrices ($C_{ext/sc}^k(\lambda)$ and $\mathbf{P}_k(\lambda,\vartheta)$) (Eqs. (1a)-(1c)).

Due to limited information content of passive remote sensing instruments to the detailed atmosphere vertical structure, the microphysical aerosol properties (and as a result total optical properties) in TROPOMI/GRASP approach are considered to be the same at different vertical levels and only the total concentration $c_v(z)$ is changed vertically, approximated by exponential probability density function $f_{pdf}^{aer}(z)$:

$$k_{ext}^{aer}(z,\lambda) = c_v(z)C_{ext}^{aer}(\lambda), c_v(z) = c_v^{(0)} f_{pdf}^{aer}(z), k_{ext}^{aer}(z,\lambda) = \tau_{ext}^{aer} f_{pdf}^{aer}(z), \tag{2a}$$

$$f_{pdf}^{aer}(z) = \frac{1}{Z_{norm}^{aer}} \, exp\left(-\frac{z}{z_{aer}}\right), \tag{2b}$$

$$\int_{Z_{min}}^{Z_{max}} f_{pdf}^{aer}(z)dz = 1. \tag{2c}$$

$k_{ext}^{aer}(z)$ is aerosol extinction profile, Z_{min} and Z_{max} are bottom (ground level) and top of atmosphere vertical levels. Z_{norm}^{aer} is normalization height, which is equal to aerosol characteristic height z_{aer} ($Z_{norm}^{aer} = z_{aer}$) for the case when $Z_{min} \ll z_{aer}$ and $Z_{max} \gg z_{aer}$.

Neglecting gas absorption in atmosphere, the total phase matrix $\mathbf{P}$ as well as extinction and scattering coefficients (k_{ext} and k_{sc}) at each vertical level z of atmosphere can be represented as combination of aerosol and Rayleigh optical characteristics:

$$k_{ext}(z,\lambda) = k_{ext}^{aer}(z,\lambda) + k_{ext}^{R}(z,\lambda), \tag{3a}$$

$$\omega(z,\lambda)\mathbf{P}(z,\lambda,\vartheta) = \frac{\omega^{aer}(\lambda)\mathbf{P}^{aer}(\lambda,\vartheta)k_{ext}^{aer}(z,\lambda) + \mathbf{P}^{R}(\lambda,\vartheta)k_{ext}^{R}(z,\lambda)}{k_{ext}^{aer}(z,\lambda) + k_{ext}^{R}(z,\lambda)}, \tag{3b}$$

where $\mathbf{P}^R$ and $k_{ext}^R(z,\lambda)$ are Rayleigh scattering matrix and extinction coefficient. The later can be well described by exponential vertical probability density function with characteristic height z_R:

$$k_{ext}^{R}(z) = \tau_{ext}^{R} f_{pdf}^{R}(z), \tag{4a}$$

$$f_{pdf}^{R}(z) = \frac{1}{z_{norm}^{R}} \, exp\left(-\frac{z}{z_R}\right), \tag{4b}$$

$$\int_{Z_{min}}^{Z_{max}} f_{pdf}^{R}(z)dz = 1. \tag{4c}$$

Eq.(3b) shows that even assuming vertically independent aerosol optical properties (Eq.(1a)-(1c)) the total phase matrix and SSA are still vertically dependent at the wavelengths where the contribution of Rayleigh scattering is considerable. Since Rayleigh vertical profile (Eqs. (4a)-(4c)) is well-known globally and, usually, is very different from aerosol one ($z_R \neq z_{aer}$, Eqs.(2a)-(2c), 4(a)-4(c)), the spectral dependence of the atmospheric vertical scattering profile (Eq.(3b)) can provide some sensitivity to the aerosol vertical profile. Having been performed in the

range from UV (with strong Rayleigh scattering contribution) to NIR and SWIR (negligible Rayleigh scattering), the TROPOMI/GRASP retrieval can be affected by the vertical aerosol profile. Therefore, together with the total column volume concentration $c_v^{(0)}$ and four relative fractions for each aerosol component c_k, the aerosol characteristic height z_{aer} of the exponential vertical profile is also retrieved in the TROPOMI/GRASP approach. Despite its potential value, the accuracy of such aerosol height characterization from the TROPOMI/GRASP UV, VIS, NIR and SWIR retrievals still requires detailed analysis and validation, and it is not considered in this paper.

4.1.2. Surface BRDF model

The multiple scattering in atmosphere as well as surface atmosphere coupling may result in essential manifestation of the polarized scattered light even in radiance only measurements. The effect can be noticeable when the contribution of Rayleigh and aerosol scattering with high degree of polarization is essential in the multiple scattering. Therefore, Vector Radiative Transfer (VRT) code was used in TROPOMI/ GRASP processing, where surface reflection is described by the surface Bidirectional Reflection Matrix (BRM) whose element R11 is directedly related with Bidirectional Reflectance Distribution Function (BRDF).

4.1.2.1. BRM model over land. Over land, GRASP has a wide variety of surface reflection models: semi-empirical Rahman–Pinty–Verstraete (RPV) model, kernel-driven counterparts (Ross–Li and Ross–Roujean models (Ross, 1981; Li and Strahler, 1992; Wanner et al., 1995)) their modifications or more physically-based models (Maignan et al., 2009; Litvinov et al., 2011a, 2011b).

An extensive comparison of different land BRDF models showed their good abilities to describe adequately airborne and satellite measurements (Maignan et al., 2004; Litvinov et al., 2011a, 2011b). For TROPOMI/GRASP processing over land, the Ross-Li sparse model (Ross, 1981; Li and Strahler, 1992) was used as land BRDF model with additional hot spot effect correction (Maignan et al., 2004) and the constraints on BRDF model parameters spectral variability as described in (Litvinov et al., 2011a, 2011b). Despite the fact that the other models were performing comparably well, the modified Ross-Li model was specifically selected for this study due to the following reasons: (i) the model can be represented as a linear combination of the kernels, resulting in a linear dependence of the surface reflectance on the retrieved BRDF parameters; (ii) the calculations of the surface reflectance with the Ross-Li BRDF model are fast; (iii) the model is well-known and widely used, which simplifies the intercomparison with other available surface products from different satellites (Schaaf et al., 2002; Wang et al., 2018; Lyapustin et al., 2018).

Over land the total surface reflectance matrix ($\mathbf{R}_{sur}^{land}$) in TROPOMI/GRASP processing is modelled as the following:

$$\mathbf{R}_{sur}^{land} = \begin{pmatrix} R_I & 0 & 0 & 0 \\ 0 & 0 & 0 & 0 \\ 0 & 0 & 0 & 0 \\ 0 & 0 & 0 & 0 \end{pmatrix}, \tag{5}$$

$$R_I = \pi \bullet BRDF \tag{6}$$

Here R_I is the total surface reflectance related to Bidirectional Reflectance Distribution Function (BRDF).

Although TROPOMI/GRASP processing is based on VRT, the elements of the reflectance matrix describing land surface polarization are not considered in Eq. (5). First of all, this is due to the fact that the degree of polarization for land surfaces is usually rather modest and, as a result, the effect of surface polarized components on the top of atmosphere total reflectance (which is due to atmosphere-surface coupling) is negligible for the majority of land surface types. Second, most of the widely used models for surface total and polarized reflectance description are semi-empirical, with parameters that are not related to each other (Ross, 1981; Li and Strahler, 1992; Maignan et al., 2009; Litvinov et al., 2011a, 2011b). Therefore, introducing Bidirectional Polarization Distribution Function (BPDF) into the total surface BRM (Eq. (5)) would increase the number of retrieved parameters, resulting in additional uncertainties of the retrieval when radiance-only measurements are available. In general, full surface BRM with non-zero polarization elements in Eq. (5) is crucial only for polarimetric measurements, for example, from POLDER/PARASOL or future space-borne polarimeters (e.g., 3MI, CO2M MAP, etc. Dubovik et al., 2019).

Ross-Li BRDF used to simulate the surface reflectance in the TROPOMI/GRASP processing can be presented as the linear combination of three kernels a_{iso}, f_{vol}, and f_{geom} representing isotropic, volumetric, and geometric optics surface scattering, respectively (Roujean et al., 1992; Li and Strahler, 1992; Wanner et al., 1995). To account for essential increasing in land surface reflectance near backscattering direction, the "hot spot" effect correction was used (Maignan et al., 2009). Moreover, based on the studies performed in (Litvinov et al., 2010, 2011a, 2011b) this model is presented in the renormalized form as following:

$$R_I = \pi \bullet BRDF = a_{iso}(\lambda)\Big(1 + a_{vol}f_{vol}(\vartheta_0, \vartheta_v, \Delta\varphi) + a_{geom}f_{geom}(\vartheta_0, \vartheta_v, \Delta\varphi)\Big), \tag{7}$$

$$f_{vol}(\vartheta_0, \vartheta_v, \Delta\varphi) = f_{HotSp}(\gamma)\frac{(\pi/2 - \gamma)cos\gamma + sin\gamma}{cos\vartheta_0 + cos\vartheta_v} - \frac{\pi}{4}, \tag{8}$$

$$f_{HotSp}(\gamma) = 1 + \frac{1}{(1 + \pi - \gamma)/\alpha_0}, \alpha_0 = 1.5. \tag{9}$$

where ϑ_0, ϑ_v are solar and viewing zenith angles, $\Delta\varphi$ is the difference of viewing and solar azimuth angles, γ is the scattering angle. The f_{geom} kernel in Eq. (7) is the same as in original paper by Li and Strahler (1992). It can be also found in number of other papers (Maignan et al., 2004; Litvinov et al., 2011a, 2011b) and is not described here in details.

On the basis of analysis of Research Scanning Polarimeter (RSP) polarimetric measurements over soil and vegetated surfaces in VIS and SWIR range, it was shown that for the same surface type BRDF angular shape can be considered approximately spectrally invariant in the wide range of illumination and scattering geometries (Litvinov et al. (2010, 2011a and 2011b)). This spectral invariance of the BRDF angular shape is related to the weaker spectral variability of the second (a_{vol}) and third (a_{geom}) BRDF parameters in comparison to the first one $a_{iso}(\lambda)$ when Ross-Li model is renormalized like in Eq. (7).

The spectral invariance of BRDF angular shape for the same surface type (i.e. the linear spectral dependence of BRDF (Eq.(7)) was extrapolated also to UV and deep blue channels in the TROPOMI/GRASP processing. Such assumption reduces the number of retrieved parameters, which is crucial for the retrieval of measurements with limited information content. The studies performed in the frame of the ESA S5P + I AOD/BRDF project demonstrated more accurate and stable results both for aerosol and surface retrieval when the second (a_{vol}) and third (a_{geom}) BRDF parameters in Eq. (7) are considered to be spectrally independent (TROPOMI, 2022b).

4.1.2.2. BRM model over sea/ocean. Sea/ocean reflection description in TROPOMI/GRASP processing incorporates different approaches accounting for surface reflection and scattering. In particular, the specular Fresnel reflection from rough Gaussian surfaces is described with the Cox and Munk model (Cox and Munk, 1954), taking into account the shadowing effect (Tsang et al., 1985; Mischenko and Travis, 1997). The water leaving reflectance as well as foam/whitecaps reflectance were assumed isotropic (Voss et al., 1996) and modelled in Lambertian approximation. The relations between whitecaps/foam fraction and wind speed are defined by the empirical formula by Monahan and O'Muircheartaigh (1980). The spectral dependence of foam is accounted with the model described in (Frouin et al., 1996; Frouin and Pelletier, 2015).

In general, the reflection matrix over water surfaces ($\mathbf{R}_{sur}^{water}$) is represented as follows:

$$\mathbf{R}_{sur}^{water} = \delta_{Fr} f_{shad}(\vartheta_0, \vartheta_v)\mathbf{R}_{CoxM}(\vartheta_0, \vartheta_v, \Delta\varphi; m, \sigma^2) + r_0(\lambda), \quad (10)$$

$$\mathbf{R}_{CoxM} = \frac{\mathbf{R}_{Fr}(m, \vartheta_0, \vartheta_v, \Delta\varphi, \gamma)}{2\pi\mu_n^2\sigma^2} exp\left(-\frac{1-\mu_n^2}{\mu_n^2 2\sigma^2}\right), \quad (11)$$

$$\mu_n = \frac{cos\vartheta_0 + cos\vartheta_v}{|\mathbf{n}_v + \mathbf{n}_0|},$$

$$\mathbf{n}_0 = (sin\vartheta_0 cos\varphi_0; sin\vartheta_0 sin\varphi_0; cos\vartheta_0),$$

$$\mathbf{n}_v = (sin\vartheta_v cos\varphi_v; sin\vartheta_v sin\varphi_v; cos\vartheta_v),$$

$$f_{shad}(\vartheta_0, \vartheta_v) = \frac{1}{1 + f_{1shad}(\vartheta_0, \sigma) + f_{1shad}(\vartheta_v, \sigma)}, \quad (12)$$

$$f_{1shad}(\vartheta_v, \sigma) = \sqrt{\frac{2}{\pi}}\sigma\sqrt{\frac{1-\mu^2}{2\mu}} exp\left(\frac{\mu^2}{2\sigma^2(1-\mu^2)}\right) - erfc\left(\frac{\mu}{\sigma\sqrt{2(1-\mu^2)}}\right), \quad (13)$$

$$\mu = cos\vartheta,$$

$$r_0(\lambda) = (1-\delta_{Fr})r_{WhC}(\lambda) + \delta_{Fr} r_w(\lambda), \quad (14)$$

$$\delta_{Fr} = 1 - \delta_{WhC}, \delta_{WhC} = \left(2.95 \bullet 10^{-6} W^{3.52}\right), \quad (15)$$

$$2\sigma^2 = 0.003 + 0.00512W, \quad (16)$$

$$r_{WhC}(\lambda) = r_{WhC}^{440} exp\left(-1.75(\lambda_{\geq 0.6} - 0.6)^{0.99}\right), r_{WhC}^{440} = 0.22. \quad (17)$$

Here $\mathbf{R}_{CoxM}$ is the well-known reflection matrix of the Cox and Munk model, where $\mathbf{R}_{Fr}$ is Fresnel reflection matrix from water surface facets with refractive index m (Tsang et al., 1985; Mischenko and Travis, 1997), f_{shad} is the shadowing function for Gaussian random rough surface, W is the wind speed at the surface level (Tsang et al., 1985; Mischenko and Travis, 1997), and δ_{WhC} is the fraction of surface covered by whitecaps/foam (Monahan and O'Muircheartaigh, 1980). φ_0, φ_v are solar and viewing azimuth angles ($\Delta\varphi = \varphi_v - \varphi_0$). The non-Fresnel part of the surface reflectance ($r_0(\lambda)$ in Eq. (10)) takes into account scattering by whitecaps ($r_{WhC}(\lambda)$) and in water body ($r_w(\lambda)$) (Eq. (14)). The spectral dependence of the reflectance from the surface covered by whitecaps/foam ($r_{WhC}(\lambda)$) is described by Eq. (17) according to Frouin et al. (1996).

In the TROPOMI/GRASP processing wind speed information (W in Eqs. (15) and (16)) is taken from the S5P/TROPOMI L2 dataset (see Section 2) and the spectral water body reflectance $r_w(\lambda)$ is the only retrieved parameter of the ocean model, whose variability is essentially constrained by applying GRASP single and multi-pixel constraints (Appendix 1).

4.2. Auxiliary information in TROPOMI/GRASP retrieval

Proper definition of a priori constraints is a crucial aspect in the development of efficient retrieval algorithm for any satellite measurements, suffering from the lack of information content. Similarly, suitable initiation of the initial guess often helps to optimize the satellite retrievals. Therefore, in order to identify the optimal GRASP approach, first, a series of numerical tests were conducted on a rather extensive but limited dataset of S5P/TROPOMI measurements.

The aerosol model used for the TROPOMI/GRASP retrieval is already constrained essentially by the number of the retrieval parameters (there are only five spectrally independent aerosol parameters as discussed in Section 4.1.1). One of the biggest uncertainties in aerosol and surface characterization is related to the accurate separation of aerosol and surface signals. In general, surface BRDF models used in the TROPOMI/GRASP retrieval both over land and ocean contain twelve retrieval parameters (ten of them are spectrally dependent and two are independent of wavelength as described in Section 4.1.2). Therefore, for ordinary single pixel retrieval a priori information about surface parameters is necessary to constrain the solution of the inverse problem. Among well-known approaches, such a priori information may be based on an external surface database, when the variability of the surface BRDF parameters is constrained either directly by a priori values from climatology or by using a priori known spectral ratios of BRDF (Strahler et al., 1999; Vermote and Kotchenova, 2008).

The effects of different surface reflectance a priori constraints and initial guess definition on the TROPOMI/GRASP retrieval were evaluated for the following cases: (i) full BRDF retrieval when all model parameters are retrieved; (ii) KNMI DLER TROPOMI climatology (Tilstra et al., 2017, 2021, 2024) is used as initial guess for first BRDF parameter; (iii) POLDER/GRASP BRDF climatology as a priori estimates for the 2nd (volumetric) and 3rd (geometric) BRDF parameters is applied; (iv) ECMWF wind speed at surface boundary level is used as a priori estimates for the GRASP ocean model (Section 4.1.2.2).

After a series of tests ((i) - (iii)) with TROPOMI data over land, it was found that the usage of direct a priori estimates for surface BRDF parameters is not crucial, and stable retrieval of aerosol properties can be obtained using proper "single-pixel" and "multi-pixel" smoothness constrains (Table A1) in the GRASP algorithm (Fig. 1).

Sea/ocean BRDF parameters (δ_{Fr} and σ^2 in Eqs. (14)–(16)) depend on the wind speed. The wind speed can change very fast during a day as well as from day to day resulting in essential variability of sea/ocean BRDF parameters. Therefore, applying multi-pixel constraints over sea/ocean may not be as efficient as over land to separate aerosol and ocean signals, especially close to the glint direction where water surfaces become very bright. This logical conclusion was confirmed by TROPOMI/GRASP retrieval tests performed without and with wind information (test (i) and (iv)). In particular, it was found that over water surfaces, constraints of the second and the third water BRDF parameters (δ_{Fr} and σ^2) by a priori estimates using wind speed may be very important for aerosol retrievals, especially near in the vicinity of glint direction (Fig. 2).

The test results on sensitivity to various a priori constraints over land performed for S5/TROPOMI show crucial differences in comparison to the results for the S3/OLCI instrument obtained with the GRASP algorithm. In particular, the utilization a priori estimates for BRDF parameters over land were found to be crucial for the OLCI/GRASP retrieval (Chen et al., 2022b) whereas the TROPOMI/GRASP retrieval is very stable, independently of the initial guess (Fig. 1). These differences in the land surface retrieval setup can be explained by the higher information content of S5P/TROPOMI measurements in comparison to S3/OLCI: (a) much wider spectral coverage of S5P/TROPOMI instrument (UV, VIS, NIR and SWIR TROPOMI measurements vs VIS and NIR OLCI measurements) and (b) wider swath provided by S5P/TROPOMI instrument in comparison to S3/OLCI (~2600 km (TROPOMI) vs ~1270 km (OLCI)). This results in better temporal, angular and spectral sampling of day-to-day measurements which are used in the GRASP multi-temporal retrieval.

The observed good performance of the TROPOMI/GRASP retrieval over land without any a priori estimates for the retrieved surface parameters allows for the generating an independent high-quality aerosol and surface products from UV to SWIR. In particular, full TROPOMI/GRASP retrieval conducted for 3 BRDF parameters is completely independent of any existent surface satellites products and associated to them uncertainties.

5. TROPOMI/GRASP extended properties retrieval

The GRASP S5P/TROPOMI product contains direct retrieved

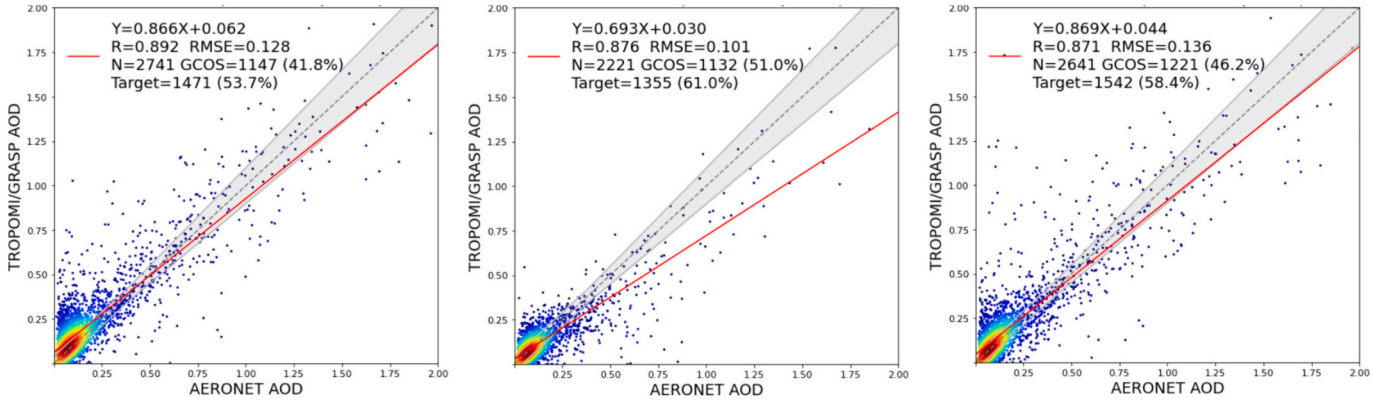

Fig. 1. TROPOMI/GRASP retrieval of aerosol properties over land vs AERONET. Left panel: the retrieval without using a priori estimates constraints (test (i)). Middle panel: initial guess from KNMI DLER TROPOMI climatology is used (test (ii)). Right panel the results obtained when a_{vol} and a_{geom} BRDF parameters are constrained by the a priori estimates from POLDER/GRASP BRDF climatology (test (iii)).

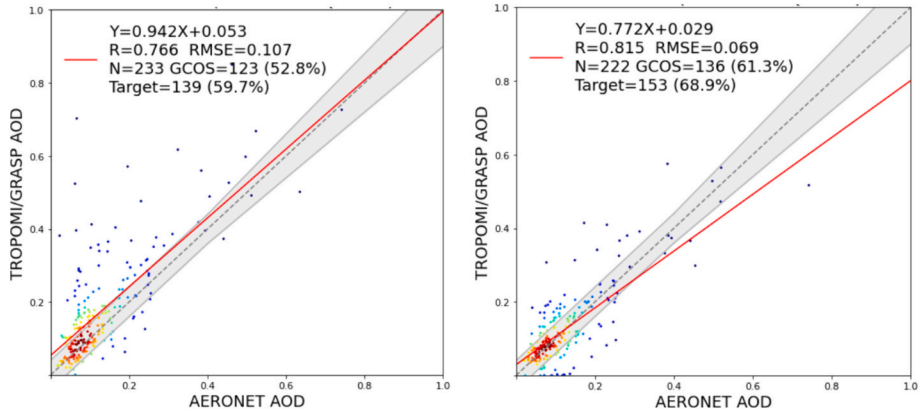

Fig. 2. TROPOMI/GRASP retrieval of aerosol properties over sea/ocean vs AERONET. Left panel: the retrieval without constraints by a priori estimates. Right panel the results obtained when 2 BRDF parameters are constrained by a priori estimates of the wind speed (Section 4.1.2.2) and the model for foam fraction (Frouin et al., 1996).

parameters (see section 4.1.1 and 4.1.2) as well as derived aerosol and surface properties (TROPOMI, 2022a).

One of the main aerosol optical product derived from satellite measurements and widely used for environment studies is the spectral AOD (noted as τ_{ext}^{aer} in Eq. (1a)), which represents the column amounts of aerosols in the atmosphere. Despite a big progress achieved in AOD retrieval from different polar orbiting and geostationary satellites (Choi et al., 2016; Govaerts et al., 2010; Hsu et al., 2013, 2019; Kikuchi et al., 2018; de Leeuw et al., 2015; Levy et al., 2013; Lyapustin et al., 2018; Sayer et al., 2018a; Thieuleux et al., 2005; Torres et al., 2007), satellite AOD characterization in general and over bright surfaces in particular should be essentially improved for the most of the algorithms to meet the climate study requirements (Table 2, GCOS, 2016).

The TROPOMI/GRASP product provides spectral AOD at 10 wavelengths from UV to SWIR (Table 1). Together with AOD, several more detailed aerosol characteristics such as spectral fine mode AOD (AODF) (the coarse mode AOD (AODC) can be obtained as AODC = AOD - AODF), AE, spectral SSA, Absorbing AOD (AAOD) are also presented in the product (the particle radius cutoff is defined at 0.6 μm to obtain AODF and AODC. These detailed aerosol characteristics are related to aerosol particle size and absorption, which are key parameters for the climate and air quality studies.

Angstrom Exponent (AE or α) represents the spectral dependence of AOD at selected wavelengths.

$$\alpha = -\frac{ln\left(\frac{AOD(\lambda_1)}{AOD(\lambda_2)}\right)}{ln\left(\frac{\lambda_1}{\lambda_2}\right)} \tag{18}$$

AE directly depends on the microphysical properties of aerosol such as the size distribution and the spectrally dependent complex refractive index. Since for the atmospheric aerosol the spectral dependence of the complex refractive index is smooth in the UV, VIS and NIR spectral range, it has minor effect on AE in comparison to the size. Therefore, AE is very often used as an indicator of domination of small or coarse particles in the observed aerosol particle mixture. For example, high values of AE (AE > ~1.3) correspond to domination of small aerosol particles (with radius below ~0.5 μm) showing strong decreasing of particles extinction cross section (and as a result, decreasing of AOD) with increasing of the wavelength (for example, from VIS and NIR spectral range). Small values of AE (for example, AE < ~0.5) correspond to aerosol mixture dominated by big particles (with radius above ~1.0 μm) with weak spectral AOD dependence. Intermediate AE values (~0.5 < AE < ~1.3) are usually associated to moderate size or mixture of small and big particles. At present time, AE characterization from satellite measurements requires essential improvement.

Single Scattering Albedo (SSA) (Eq. (1b)) values at different spectral channels strongly depend on the complex refractive index (the real and imaginary parts) and size of the particles. SSA cannot be directly measured from remote sensing measurements but can be retrieved from

them. It is one of the most challenging parameters to retrieve from remote sensing. AERONET retrieves SSA by fitting the ground-based direct sun AOD measurements and "almucantar" radiance measurements with radiative transfer modelling (Dubovik and King, 2000). It was pointed out that reliable SSA values from AERONET can be obtained for high AOD events (with AOD (440) values higher than ~0.4) while for lower AOD cases the accuracy of SSA retrieval significantly decreases (Dubovik et al., 2000). The retrieval of SSA parameter from a space-borne instrument is even more challenging problem related to different instrumental, physical and technical issues. Being one of the most crucial parameters for climate studies and air quality control, global SSA retrieval from most of the space-borne measurements is not satisfactory yet and requires essential improvement.

From AOD and SSA such aerosol characteristics as Absorption AOD (AAOD) is calculated and presented in the TROPOMI/GRASP product:

$$AAOD(\lambda) = (1 - SSA(\lambda))*AOD(\lambda) \quad (19)$$

AAOD describes the absorption part contained in total AOD and is essential additional optical parameter for aerosol absorption characterization.

An example of AOD, AE, fine mode AOD (AODF), and SSA from TROPOMI/GRASP retrieval is presented in Fig. 3.

As it was discussed above, the spectral dependence of AOD, represented by AE, provides essential information about aerosol size. On another hand, the wavelength dependence of SSA provides valuable information about the absorption properties together with size. In particular, for non-absorbing or slightly absorbing particles (when the imaginary part of the complex refractive is 0 or very small in different spectral channels) SSA is close to 1 at any wavelengths independently of the size of particles. For absorbing ones SSA shows essential spectral dependence defined both by the particles size and by the spectral dependence of particles complex refractive index. We characterize the retrieved spectral dependence of the SSA from TROPOMI/GRASP product by taken the SSA difference at two wavelengths:

$$\Delta SSA(\lambda_1, \lambda_2) = SSA(\lambda_1) - SSA(\lambda_2) \quad (20)$$

Though there are other possibilities to define SSA spectral dependence (for example, using Angstrom Exponent formula (Eq.(18)) defined for SSA in the same way as for AOD), the difference in Eq.(20) removes the possible wavelengths independent systematic bias in the SSA retrieval. Moreover, the uncertainties of ΔSSA are very easy to analyze and compare relatively expected uncertainties of the absolute values of SSA.

Fig. 4 shows two-dimensional (2D) Probability Density Function (PDF) in the space of AE and ΔSSA characteristics, derived from AERONET stations and collocated TROPOMI/GRASP pixels. Here colors from blue to red indicate increasing probability to find certain AE and ΔSSA values together in the certain 2D box. In both AERONET and TROPOMI/GRASP cases, one can clearly observe the correlation between AE and ΔSSA characteristics, which is explained by the dependence of both characteristics on the aerosol size. In general, $\Delta SSA(\lambda_1, \lambda_2)$ defined at one or few pairs of wavelengths, extends essentially the possibility of global aerosol characterization regarding their size and absorption properties. In particular, the majority of cases with AE (440–670) < ~0.7 (big aerosol particles) correspond to the cases with ΔSSA (440–670) < 0 (or, in other words, with SSA (440) < SSA (670)) (Fig.4), which is typical dependence for big particles of dust aerosol. At the same time, an essential number of pixels with AE (440–670) > ~1.5 show ΔSSA (440–670) > 0 with SSA (440) > SSA (670) which is typical for absorbing small particles (for example, biomass burning aerosol) with neutral or moderate spectral dependence of the complex refractive index at these two channels. Overall, the PDF from AERONET demonstrates a bigger dispersion than the one from TROPOMI/GRASP (Fig. 4). This is because the aerosol model in AERONET retrieval is less constrained than the "models" approach used in TROPOMI/GRASP retrieval, resulting in a bigger flexibility to different aerosol species characterization. Nevertheless, as it will be shown in the next sections, ΔSSA derived from TROPOMI/GRASP describes correctly the SSA spectral dependence for the majority of cases matched-up with AERONET.

As it was noted in Section 4.1.2.1, over land, full surface reflectance in the TROPOMI/GRASP processing is described by the Ross-Li BRDF model. Therefore, the surface parameters in TROPOMI/GRASP product are represented by isotropic spectrally dependent scaling parameters $a_{iso}(\lambda)$ as well as by spectrally independent "volumetric" a_{vol} and "geometric" a_{geom} parameters, describing angular shape of the surface reflectance. They are related to the BRDF parameters ($a_{iso}^{orig}(\lambda)$, a_{vol}^{orig}, a_{geom}^{orig}) of the Ross-Li model in original representation (Li and Strahler, 1992; Wanner et al., 1995) as follows:

$$a_{iso}^{orig}(\lambda) = a_{iso}(\lambda), a_{vol}^{orig}(\lambda) = a_{vol}a_{iso}(\lambda), a_{geom}^{orig}(\lambda) = a_{geom}a_{iso}(\lambda). \quad (21)$$

Using the retrieved BRDF parameters over land and sea/ocean such characteristics as NDVI (Normalized Difference Vegetation Index), spectral DHR (Directional Hemispherical Reflectance (or Black Sky Albedo) and spectral BHR_ISO (Isotropic Bi-Hemispherical Reflectance (or White Sky Albedo) are calculated and presented in the TROPOMI/GRASP surface product (Fig. 5).

5.1. TROPOMI/GRASP aerosol product accuracy evaluation

To assess the product performance with different quality flags TROPOMI/GRASP aerosol product was validated using ground-based AERONET dataset (Holben et al., 1998; Dubovik and King, 2000; O'Neill et al., 2003; Giles et al., 2019). The details about the TROPOMI/GRASP product quality flag specification (Quality Assurance (QA) and Extended Quality Assurance (QAExtend)) can be found in Appendix 2. We follow the same matchup strategy as Chen et al., 2020 and validate one year of the TROPOMI/GRASP product (from March 2019 till February 2020). The performance was evaluated for different QA and QAExtend indices.

Figs. 6 and 7 show the validation of AOD (550 nm) against AERONET over land and ocean, respectively. Some outliers are observed for QA≥1 over land which are, probably, associated with cloud contaminated

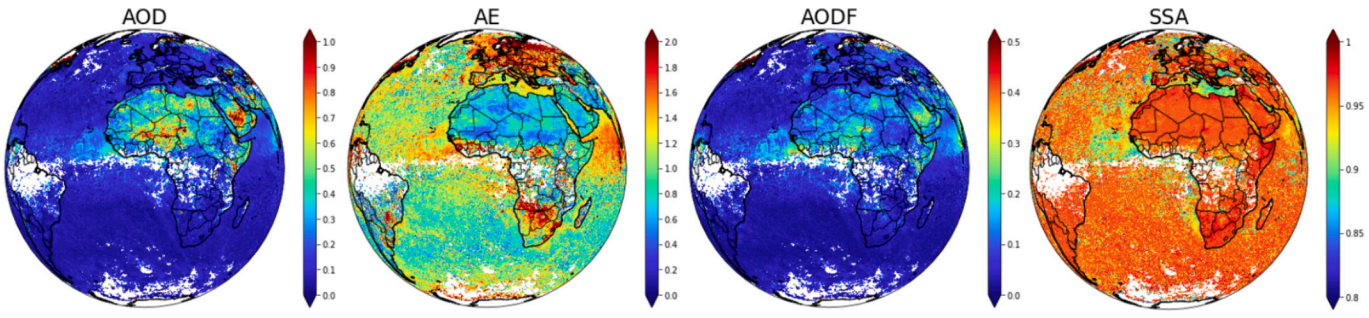

Fig. 3. Example of TROPOMI/GRASP products (April 2019) of optical aerosol characteristics at 550 nm.

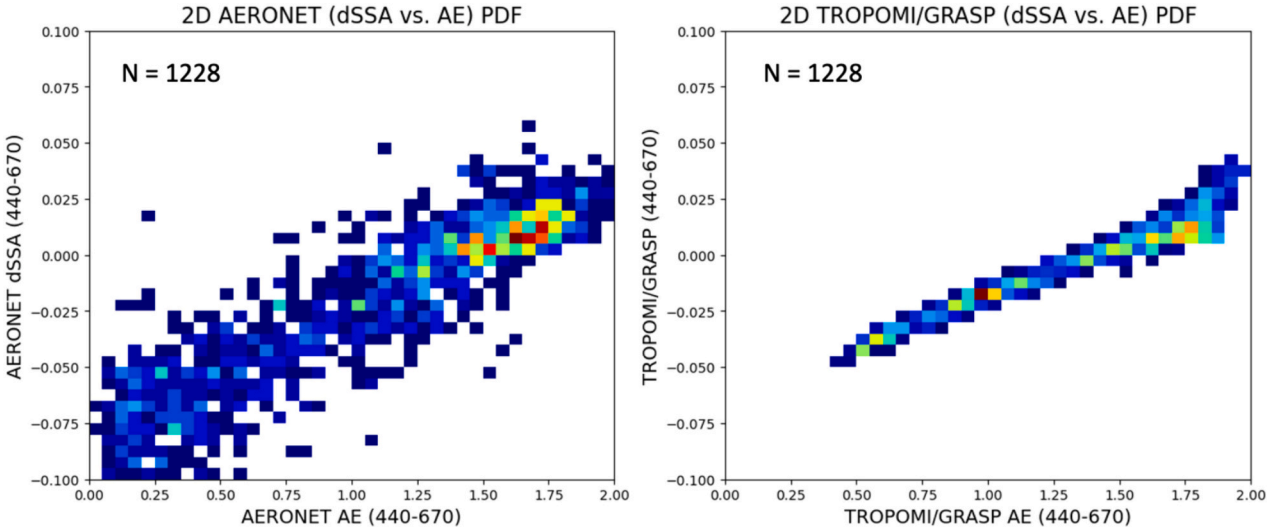

Fig. 4. 2D PDF (ΔSSA vs AE) plots from AERONET (left) and TROPOMI/GRASP (right).

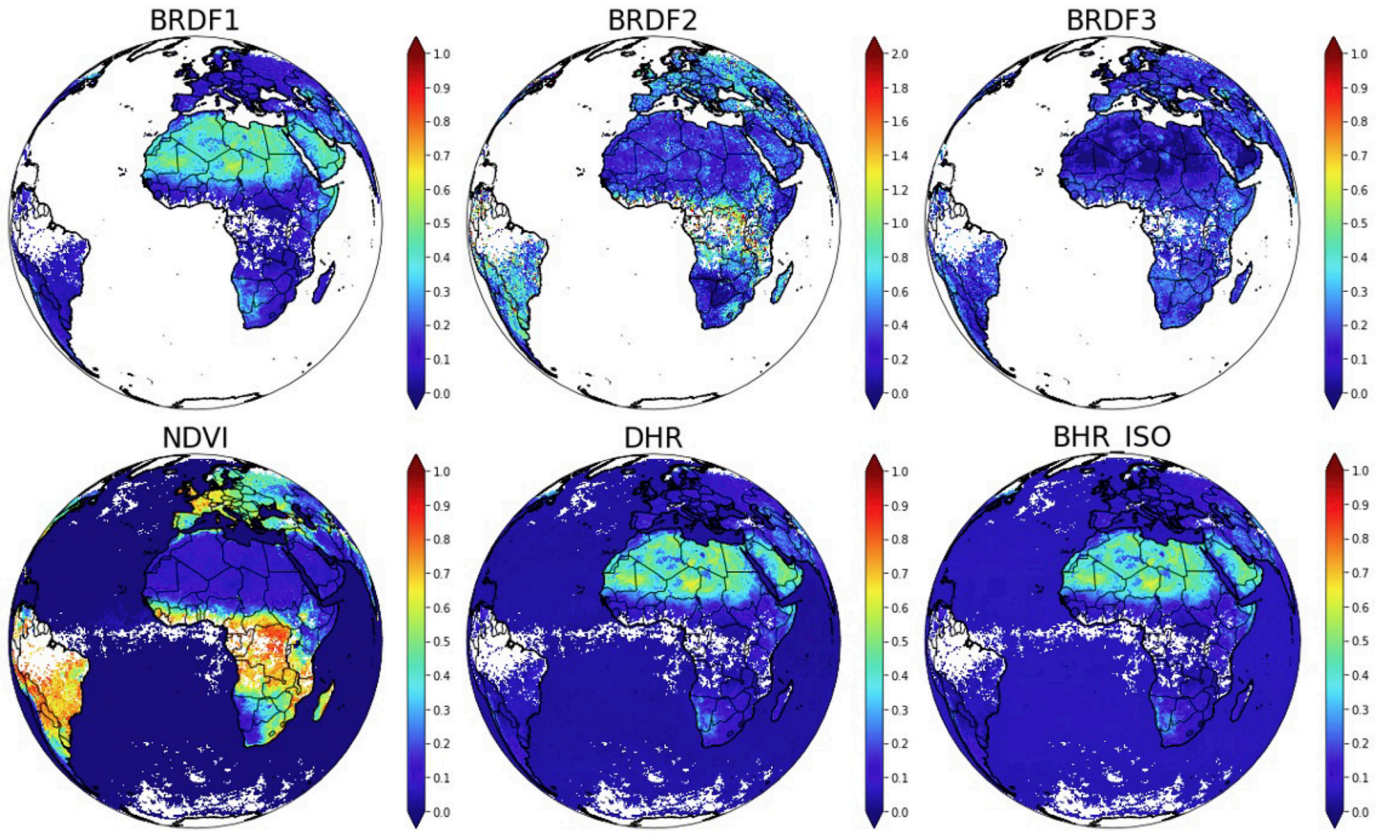

Fig. 5. Example of the TROPOMI/GRASP surface product (April 2019): BRDF1, BRDF2 and BRDF3 correspond to "isotropic" ($a_{iso}(\lambda)$), "volumetric" (a_{vol}) and "geometric" (a_{geom}) BRDF parameters, respectively. NDVI, DHR and BHR_iso correspond to Normalized Difference Vegetation Index, Directional Hemispherical Reflectance (Black Sky Albedo) and isotropic Bi-Hemispherical Reflectance (White Sky albedo).

pixels, and most of them can be screened out if QA≥2 filter is applied. Even though the validation metric for QA = 3 (R = 0.885 (Pearson correlation coefficient), RMSE = 0.078 (Root Mean Square Errors), GCOS = 56.9% (fulfilment of the "optimal" GCOS-based requirements (Table 2)), BIAS = 0.01 (average bias)) outperforms the one for QA≥2 (R = 0.833, RMSE = 0.109, GCOS = 48.4%, BIAS = 0.03), both QA≥2 and QA = 3 show good agreement with AERONET over land. Over ocean, all 3 categories (QA≥1, QA≥2 and QA = 3) show consistent performance with R ~ 0.87, RMSE ~0.05. In general, for most of the applications quality assurance index QA≥2 over land and QA≥1 over sea/ocean should be sufficient to select good quality AOD retrieval results. In the case if the best AOD performance is required, we recommend selecting pixels with QA = 3 over land and QA≥2 over ocean.

Table 3 summarizes the TROPOMI/GRASP AODF (550 nm) and AODC (550 nm) validation metrics with AERONET SDA products (O'Neill et al., 2003) over land and ocean for QA≥1, QA≥2 and QA = 3.

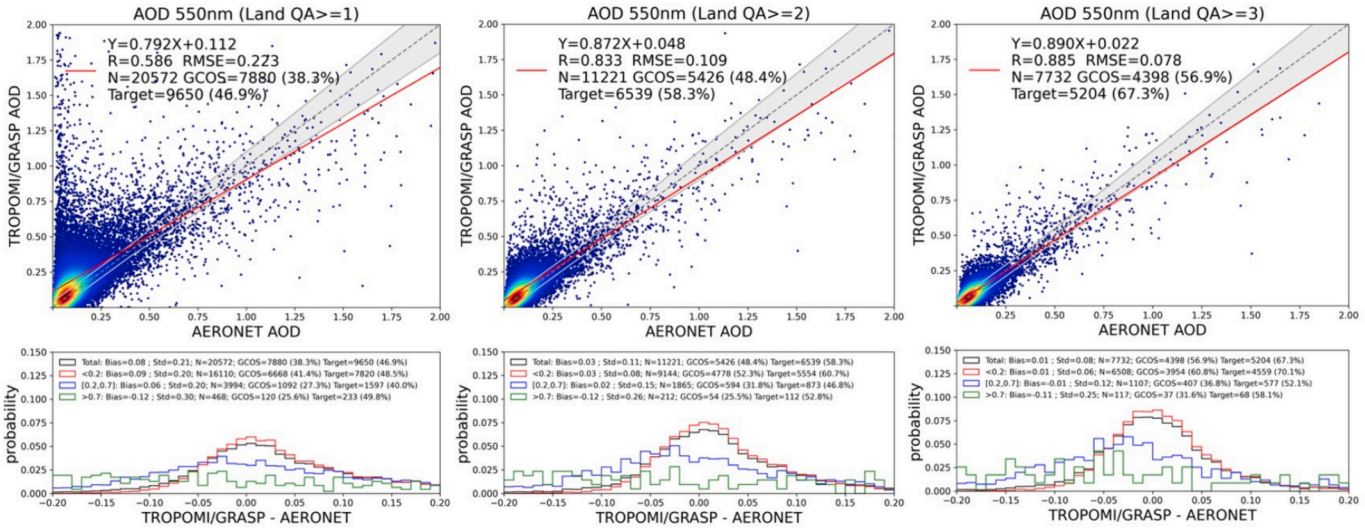

Fig. 6. Validation of TROPOMI/GRASP AOD 550 nm over land with AERONET for an entire year (March 2019 to February 2020) from left to right: QA≥1, QA≥2 and QA≥3.

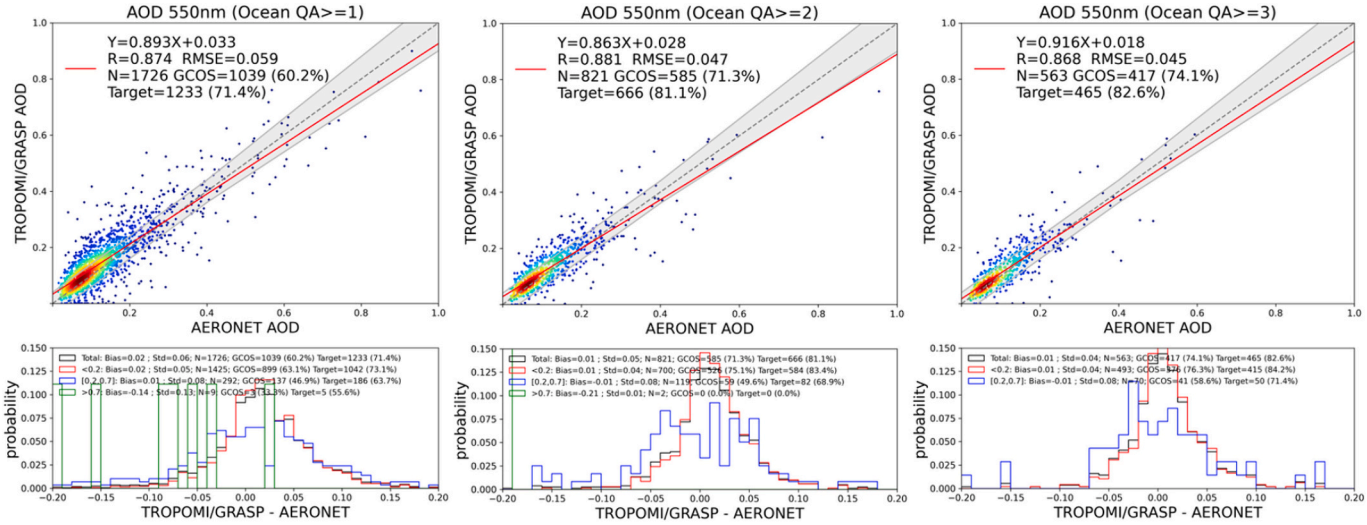

Fig. 7. The same as Fig. 6, but for AOD (550 nm) over ocean.

Table 3
Summary of TROPOMI/GRASP AODF (550 nm) and AODC (550 nm) validation metrics with AERONET SDA products over land and ocean for QA≥1, QA≥2 and QA≥3

Parameters	Land/Ocean	QA	R	Slope	Intercept	RMSE	BIAS	Target (%)	GCOS (%)
AODF (550 nm)	Land	≥ 1	0.664	0.689	0.075	0.132	0.04	56.2	48.3
		≥ 2	0.835	0.732	0.044	0.080	0.02	60.1	68.2
		≥ 3	0.851	0.763	0.028	0.062	0.01	75.7	67.5
	Ocean	≥ 1	0.748	0.776	0.037	0.061	0.02	75.2	68.7
		≥ 2	0.816	0.929	0.016	0.040	0.01	84.9	80.1
		≥ 3	0.775	0.885	0.018	0.041	0.01	84.6	78.8
AODC (550 nm)	Land	≥ 1	0.378	0.669	0.056	0.130	0.04	68.4	63.1
		≥ 2	0.627	0.711	0.025	0.062	0.01	79.9	74.9
		≥ 3	0.713	0.665	0.014	0.045	0.00	88.0	84.1
	Ocean	≥ 1	0.758	0.450	0.028	0.047	0.00	88.0	83.5
		≥ 2	0.813	0.441	0.023	0.036	0.00	93.4	90.6
		≥ 3	0.767	0.459	0.020	0.027	0.00	96.1	93.6

Similar to total AOD over land, QA≥1 products contain some clear outliers both for AODF and AODC resulting in bias around 0.04, and both QA≥2 and QA = 3 show stable results. Over sea/ocean, QA≥1 performs reasonably for both AODF and AODC.

As described in Appendix 2, for extended aerosol characteristics such as AE and SSA, and the relative fractions for each aerosol component c_k (Eqs. (1)–(4)) the quality flag for extended parameters (QAExtend) is used. Figs. 8 and 9 show validation results over land and ocean, respectively, for the TROPOMI/GRASP AE defined at two spectral bands 412 nm and 670 nm for the different values of extended quality

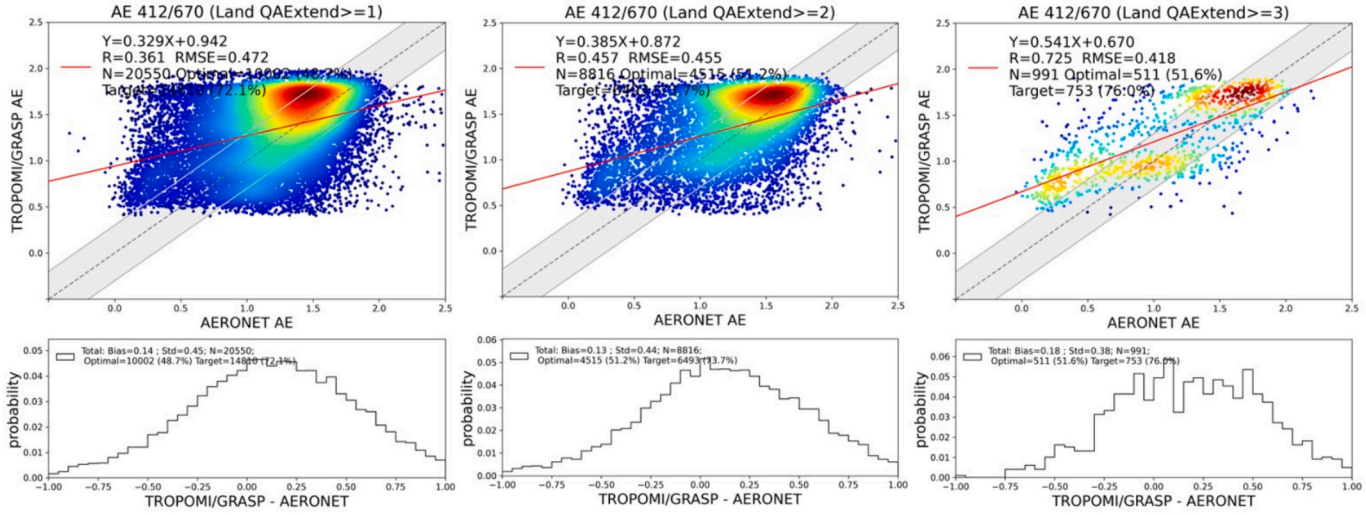

Fig. 8. Validation of TROPOMI/GRASP AE (412/670) over land with AERONET for an entire year (March 2019 to February 2020) from left to right: QAExtend≥1, QAExtend≥2 and QAExtend≥3.

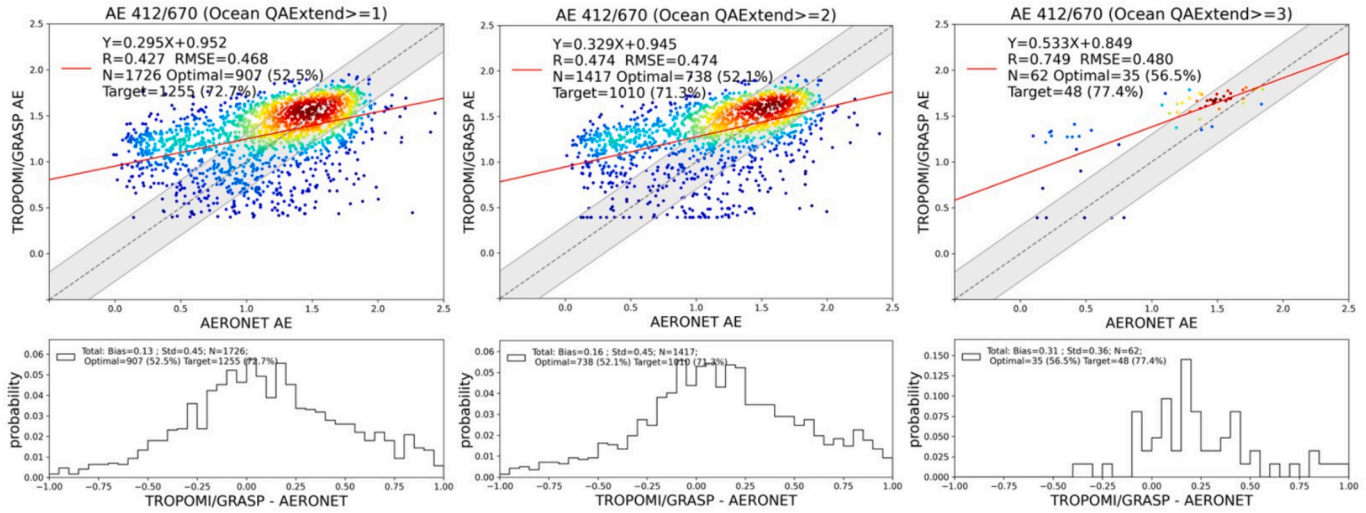

Fig. 9. The same as Fig. 8, but for AE (412/670) over ocean.

assurance index (QAExtend≥1, QAExtend≥2 and QAExtend≥3).

Over land, the QAExtend≥1 and QAExtend≥2 show similar validation results with slight improvement for correlation coefficient (R) and Root Mean Square Error (RMSE) for QAExtend≥2. For validation purposes of AE, we recommend selecting the pixels with QAExtend≥3 where the RMSE is around 0.42 and the fulfilment of AE Target requirement (±0.5, Table 2) is around 76%. For such pixels AE parameter clearly allows distinguishing between small, moderate, and large aerosol particles as demonstrated in Fig. 8 (QAExtend≥3) with three aerosol AE clusters: AE > 1.3 (small particles), 0.5 < AE < 1.3 (moderate size particles) and AE < 0.5 (large particles), respectively. AE for pixels over land with QAExtend≥2 can be rather used for qualitative analysis, allowing to distinguish small and large aerosol particles in most cases.

Over ocean, due to the filtering for aerosol loading (AOD (670) > 0.2), only 62 matchups with AERONET are found for pixels with QAExtend≥3 (Fig. 9). Nevertheless, the pixels with QAExtend≥1 and QAExtend≥2 over sea/ocean show reasonable statistics with high percentage of fulfilment of "optimal" and "target" requirements for AE. Therefore, to keep balance between the number of available pixels and quality of the retrieval, over sea/ocean we recommend using the pixels with values QAExtend≥1 or QAExtend≥2 for AE.

The performance of AE is strongly defined by correct retrieval of the aerosol component relative fractions c_k (Eq. (1)). Therefore, the recommendation for AE provided above can be applied also for selection of the pixels with meaningful relative fractions of aerosol components c_k.

Observed underestimation of particle size (overestimation of AE in Figs. 8 and 9) is similar to the POLDER and OLCI results for AE (Chen et al., 2020, 2022b), obtained also with GRASP "aerosol models" approach, described in Section 4.1.1. Potentially, the size characterization can be improved by further elaborating the "aerosol models" approach specifically for treatment of the coarse aerosol particles.

Fig. 10 shows the validation of TROPOMI/GRASP SSA at 550 nm with AERONET for different QAExtend flags. Because the AERONET Level 2 inversion products are provided only for AOD (440 nm) > 0.4 cases to ensure high accuracy SSA retrievals (Dubovik et al., 2000; Sinyuk et al., 2020), the number of matchups is very small over ocean. Therefore, the land and ocean matchups are combined in Fig. 10. In addition, the TROPOMI/GRASP product does not provide information at mid-visible 550 nm and we interpolate AOD and AAOD to 550 nm using AE and AAE from 440 nm to 670 nm and then derive SSA at 550 nm. Overall, a good agreement is observed between TROPOMI/GRASP and

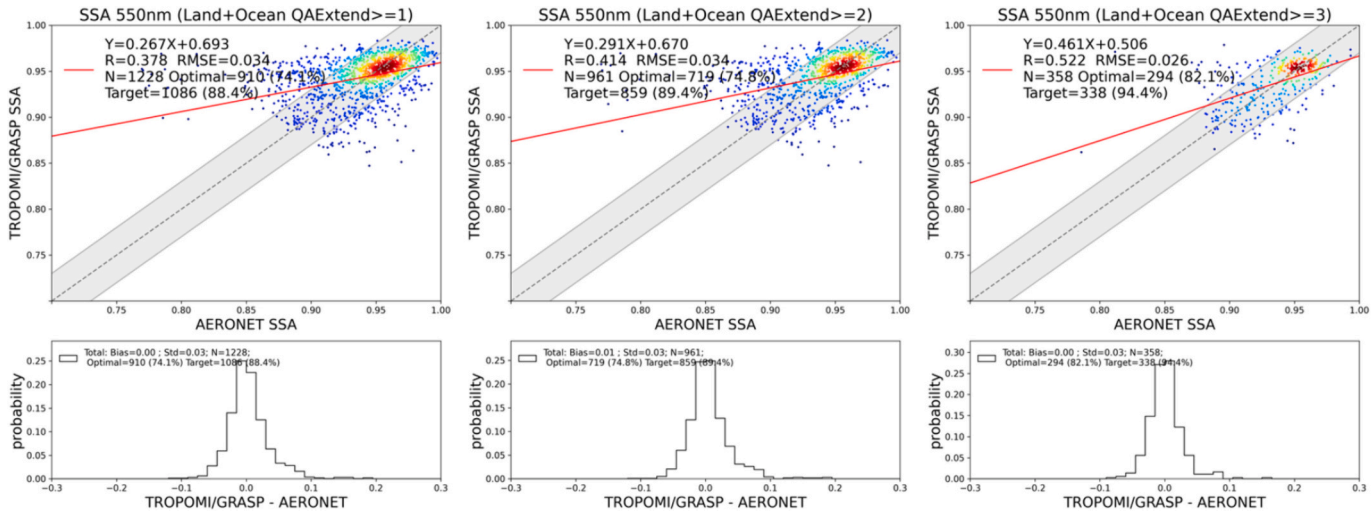

Fig. 10. The same as Fig. 8, but for SSA (550 nm) over land and ocean.

AERONET SSA with RMSE around 0.03 and >74% pixels satisfy the SSA "Optimal" requirement (±0.03) for all QAExtend indices.

Fig. 11 presents the validation of ΔSSA taken at 440 and 670 nm from the TROPOMI/GRASP SSA product versus the one calculated from AERONET SSA for the same pair of the wavelengths.

Being compared with AERONET, ΔSSA from TROPOMI/GRASP shows correct spectral dependence for most of the matched-up cases. In particular, for >75% cases both products show either increasing of SSA from blue to red spectral channel (ΔSSA (440–670) < 0) or its decreasing (ΔSSA (440–670) > 0) (Fig. 11). The performance of ΔSSA looks stable for different extended quality index values: (i) 75.8% of correct cases for spectral SSA dependence when QAExtend≥1 and 78.7% correct spectral dependencies cases for QAExtend≥3; (ii) the statistic characteristics (correlation coefficient (*R*), RMSE, slope of linear fit etc.) are very much comparable for different values of extended quality index (Fig. 11). Taking into account that the number of available pixels for analysis increase dramatically for lowest value of extended quality index (1228 match-up cases for QAExtend ≥1 vs 358 cases for QAExtend ≥3), the value QAExtend≥1 is recommended to be used when spectral dependence of SSA from TROPOMI/GRASP product is analyzed.

The correlation plots for Absorption AOD (Eq. (19)) at different values of quality indices (QA and QAExtend) are shown in Figs. 12 and 13.

Due to the definition of AAOD (Eq. 19), its value is always small for small AOD. In this way the uncertainties in SSA retrieval at small AOD have minor effect in global aerosol characterization using AAOD. This is well seen from the comparison of the Figs. 12 and 13. Both figures demonstrate similar statistic metrics of AAOD validation for QA and QAExtend indices but bigger number of matched up cases with QA index usage. Therefore, we recommend using the QA quality index to select pixels with the reliable AAOD values.

The general recommendations on the usage of the TROPOMI/GRASP aerosol product are summarized in Tables 4 and 5.

5.2. *TROPOMI/GRASP surface product accuracy evaluation*

For >20 years ground-based direct sun AOD measurements and inversion products, AERONET are used as main validation dataset for satellite aerosol retrieval (Holben et al., 1998). At present, no global and robust reference dataset for surface validation exist. This makes the validation of the surface product derived from space-borne measurements much more challenging problem than that for aerosol.

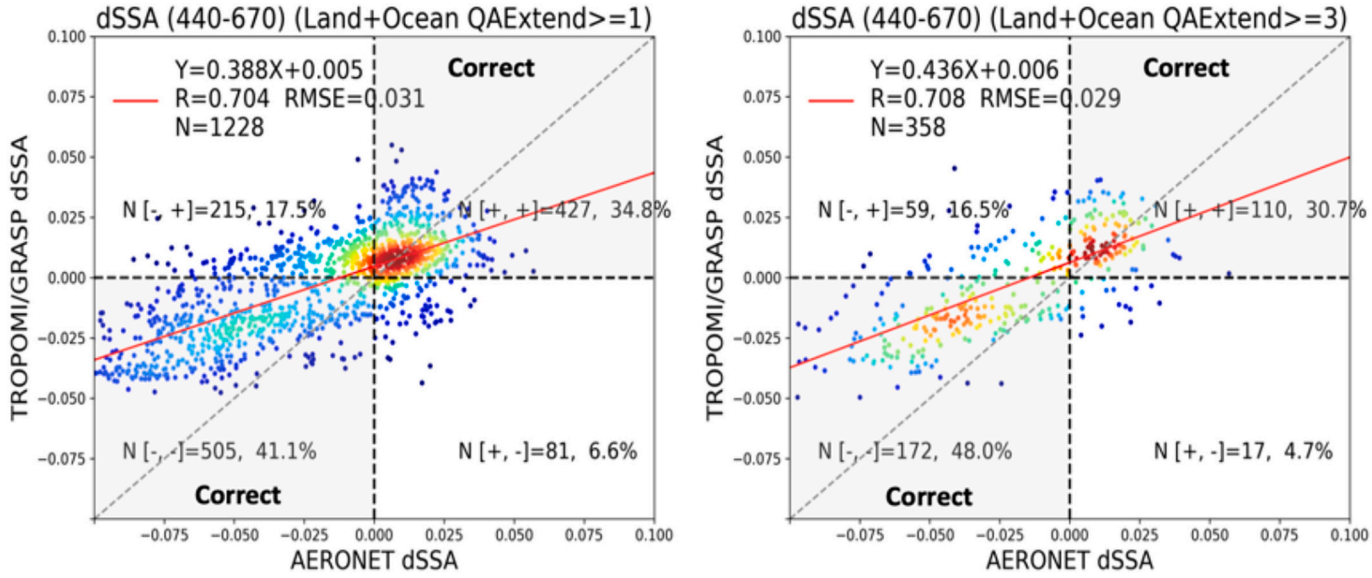

Fig. 11. ΔSSA(440–670). TROPOMI/GRASP versus AERONET.

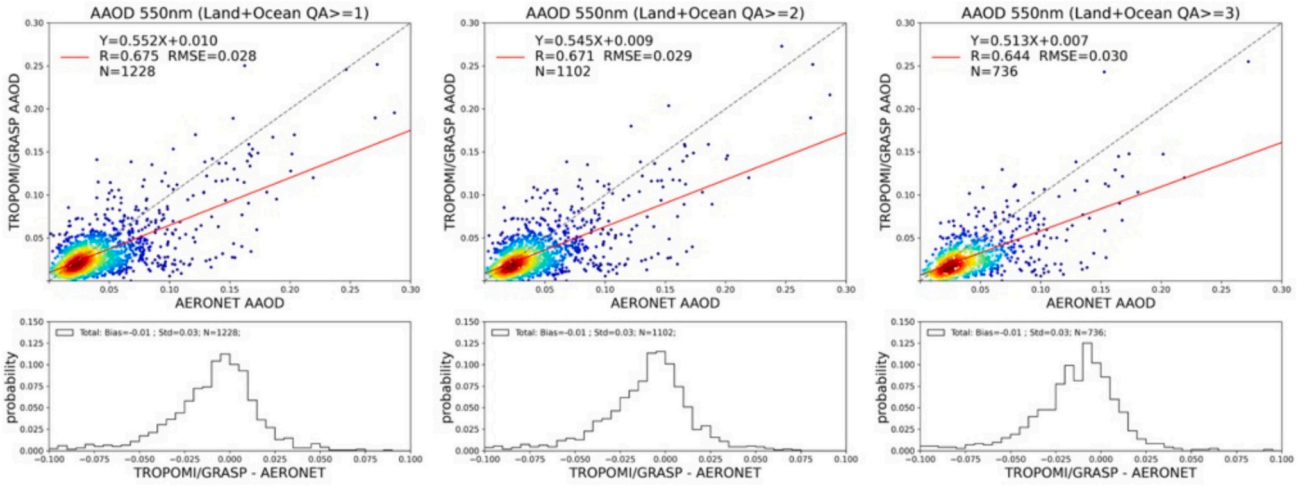

Fig. 12. Validation of TROPOMI/GRASP AAOD(550) with AERONET for an entire year (March 2019 to February 2020). From left to right: QA≥1, QA≥2 and QA≥3.

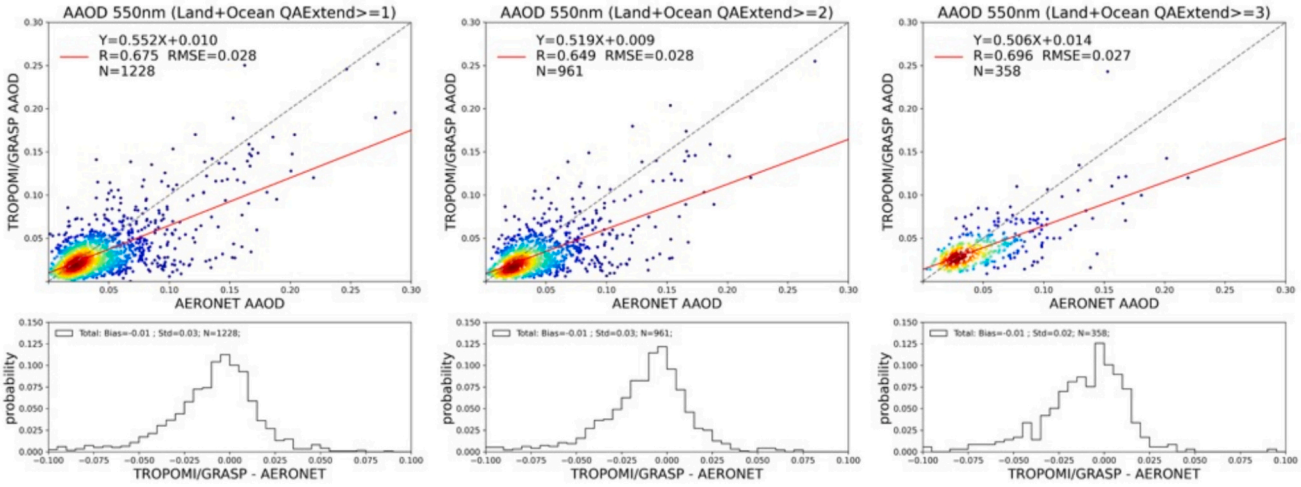

Fig. 13. The same as in Fig. 12 but for QAExtend index values.

Table 4
Quality Assurance (QA) index for the TROPOMI/GRASP AOD products.

Aerosol product	Good quality is expected		The best performance	
	Land	Ocean	Land	Ocean
AOD(λ)				
AODF(λ)				
AODC(λ)	QA≥2	QA≥ 1	QA=3	QA≥2
Total volume concentration c_v				

The surface product from the TROPOMI/GRASP retrieval was evaluated through the intercomparison with surface BRDF from the MODIS/MCD43 product (Schaaf and Wang, 2015a) as well as with recently created surface reference dataset which is based on the synergetic retrieval from combined AERONET and the S5P/TROPOMI measurements. The last one was prototyped, generated, and tested in the frame of the ESA GROSAT project (Litvinov et al., 2020; GROSAT final report: Litvinov et al., 2022) over 30 world-wide distributed AERONET stations, covering 1 year time period (from March 2019 to February 2020) and containing surface BRDF and albedos for selected the S5P/TROPOMI channels (Fig. 14).

Fig. 15 shows the validation results of the TROPOMI/GRASP albedo ("white sky" albedo or BHR_iso) against GROSAT AERONET+TROPOMI surface reference dataset (Litvinov et al., 2022). The validation was performed for all S5P/TROPOMI pixels within 30 km × 30 km area around 30 AERONET stations and for all spectral bands from Table 1.

Table 5
Quality Assurance Indices (QAExtended and QA) for the TROPOMI/GRASP extended aerosol properties.

Aerosol product	Good quality is expected		The best performance	
	Land	Ocean	Land	Ocean
AE	QAExtended ≥ 2	QAExtended≥ 1	QAExtended =3	QAExtended≥2
Aerosol component relative fraction c_k				
SSA(λ)	QAExtended ≥ 1	QAExtended ≥ 1	QAExtended ≥ 1	QAExtended ≥ 1
ΔSSA(λ_1, λ_2)				
AAOD(λ)	QA ≥2	QA ≥1	QA = 3	QA ≥2

Fig. 14. Global distribution of 30 AERONET stations from GROSAT project used for the TROPOMI/GRASP surface product validation.

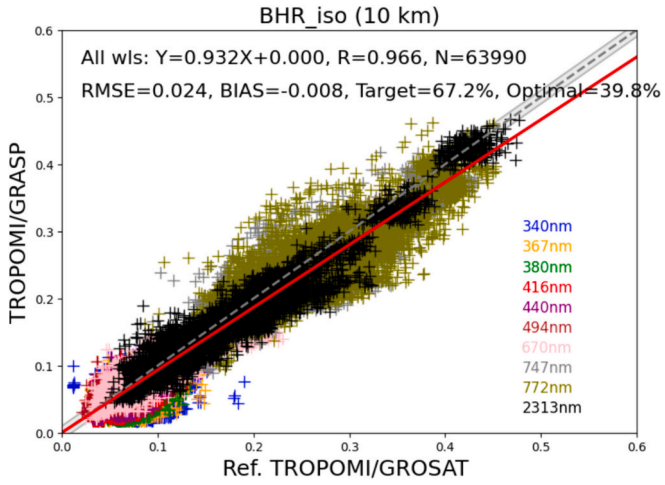

Fig. 15. Validation of TROPOMI/GRASP spectral BHR_ISO versus surface reference generated from AERONET + TROPOMI synergetic retrieval.

Overall, a good agreement is observed, for example, the correlation coefficient (R) is 0.96, bias is around −0.008, RMSE is around 0.024, and 67.2% pixels satisfy surface "Target" requirement (±0.02) formulated in Table 2. Spectrally, the RMSE is generally smaller than 0.02 at VIS channels, and slightly increases to 0.022–0.027 at UV, 0.03–0.035 at NIR and 0.022 at SWIR, which indicates the retrieval uncertainty at this level (Table 6).

Fig. 16 shows pixel-to-pixel intercomparison of MODIS/MCD43 monthly white sky albedo (Schaaf and Wang, 2015b) with TROPOMI/GRASP BHR_ISO at 670 nm for an entire year (March 2019 to February 2020) with different QA flags. More detailed global intercomparisons can be found in Part 2 of the paper (Chen et al., 2023). Overall, good agreement can be seen for all QA index values with RMSE 0.015–0.035.

Table 7 summarizes TROPOMI/GRASP surface product quality evaluation.

Table 6
Summary of statistical metrics for validation the S5P/TROPOMI GRASP spectral BHR_ISO versus GROSAT surface reference dataset for TROPOMI.

Wavelength (nm)	RMSE	BIAS (GRASP - GROSAT)	Target (%)	Optimal (%)
340	0.027	−0.009	58.8	31.8
367	0.024	−0.010	65.1	36.7
380	0.022	−0.008	68.1	38.8
416	0.019	−0.006	73.5	43.8
440	0.018	−0.006	76.2	46.0
494	0.015	−0.005	81.9	51.7
670	0.019	−0.006	75.7	49.1
747	0.031	−0.012	53.5	29.8
772	0.035	−0.013	50.1	27.6
2313	0.022	−0.009	69.4	42.5
All	0.024	−0.008	67.2	39.8

5.3. Conditions for extended aerosol/surface characterization from single-viewing observations based on TROPOMI/GRASP studies

The evaluation results show that accurate extended aerosol and full BRDF characterization can be derived from TROPOMI measurements with GRASP algorithm. Previous studies based on the application of GRASP to S3/OLCI instrument showed limited sensitivity to simultaneous full BRDF and aerosol characterization, and, in particular, the reduced quality of AE, SSA etc. of the OLCI/ GRASP retrieval (Chen et al., 2022b).

On one hand, TROPOMI/GRASP enhanced retrieval possibilities are a result of rich information content and high accuracy of S5p/TROPOMI measurements (Veefkind et al., 2012; Ludewig et al., 2020; Tilstra et al., 2020). On another hand, the big potential of such observations can be fully revealed only with the advanced retrieval and forward approaches.

Simultaneous accounting for the TROPOMI measurements from UV to SWIR spectral range in GRASP algorithm increases sensitivity to the size, concentration, absorption and scattering properties of aerosol as well as to the spectral dependence of the surface reflection. In addition, due to usually relatively small atmosphere signal in SWIR range, the spectrally neutral BRDF parameters (a_{vol} and a_{geom}, Eq.(7)) can be retrieved with enhanced accuracy in SWIR bands. Performing

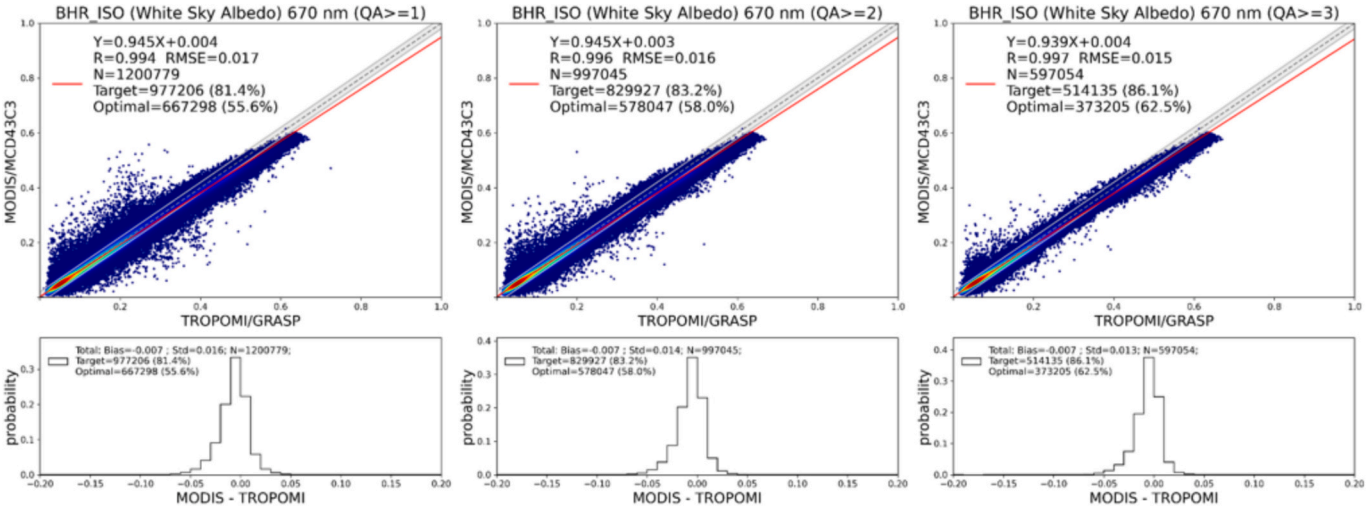

Fig. 16. Pixel-to-pixel intercomparison of MODIS/MCD43 monthly white sky albedo with TROPOMI/GRASP BHR_ISO at 670 nm for an entire year (March 2019 to February 2020) from left to right: QA ≥1, QA ≥2 and QA ≥3.

Table 7
Quality Assurance (QA) index for TROPOMI/GRASP surface properties.

Surface product	Good quality is expected		The best performance	
	Land	Ocean	Land	Ocean
Isotropic Ross-Li BRDF parameter (a_{iso})				
Isotropic Ross-Li BRDF parameter (a_{vol})				
Isotropic Ross-Li BRDF parameter (a_{geom})	QA ≥ 2	-	QA ≥ 3	-
Isotropic Bi-Hemispherical Reflectance (BHR_{iso})	QA ≥ 2	QA ≥ 1	QA ≥3	QA ≥2
NDVI				

simultaneous multi-spectral retrieval, GRASP transfers this angular surface information to UV, VIS and NIR spectral channels which improves characterization of both aerosol and surface.

TROPOMI wide swath allows almost everyday observation with different viewing zenith and azimuth angles counted for the same ground pixel. Moreover, such satellite measurements with the frequent overpassing over the same area contain information about the temporal changes of the aerosol and surface properties. Being incorporated into GRASP retrieval, the multi-temporal observations with properly applied temporal constraints result in much better surface angular properties characterization as well as more accurate differentiation between aerosol and surface signals, which, correspondingly, increases possibilities of the extended properties retrieval.

Overall, on the basis of studies of GRASP application to S5p/TROPOMI, we can conclude that combining wide spectral coverage (from UV to SWIR) and frequent revisit times (day by day or better due to wide swath of the instrument) (Section 2) with advanced algorithmic features (properly selected forward models (Section 4.1), optimized constraints (for example, spectral, multi-temporal and multi-spatial smoothness constraints (Section 4.2, Appendix 1)) one can derive extended aerosol and surface properties (Section 5) from single single-viewing radiance-only space-borne observations. Usually, such quantities are thought to be retrievable only from multi-angular instruments and especially with polarimetric measurement possibilities (Mishchenko et al., 2004; Herman et al., 1999; Hasekamp et al., 2011, 2024; Dubovik et al., 2011, 2019).

In the next section the possibilities of TROPOMI/GRASP extended characterization are demonstrated on several aerosol events in world-wide locations.

6. TROPOMI/GRASP extended aerosol characterization and aerosol events

Atmospheric aerosols show essential spatial and temporal variability in chemical and physical properties. Therefore, full aerosol characterization from remote sensing requires retrieval of such parameters as concentration, size, non-sphericity, chemical composition (complex refractive index) or related to them extended set of optical properties: AOD, AODF and AODC, AE, SSA, AAOD etc. As described above, GRASP retrieval of S5P/TROPOMI measurements provides this extended set of aerosol characteristics and their validation over AERONET stations in world-wide locations show good retrieval performance. AERONET measurements show rather typical aerosol properties which can also be observed in other locations. Therefore, being validated over AERONET stations, TROPOMI/GRASP retrieval can be used to observe and analyze a big variability of aerosol properties in other locations where ground-based measurements are not available.

In this section we use several aerosol events from the years 2019, 2020, and 2021 to demonstrate the new possibilities of aerosol characterization based on the TROPOMI/GRASP aerosol product.

Fig. 17 shows a Biomass Burning (BB) plume on September 9, 2021, originated in Spain and transported all over the Mediterranean region. Together with RGB image, Fig. 17 shows an extended set of aerosol characteristics such as AOD (440 nm), AE (AExp in the figure), ΔSSA, SSA (440 nm) and AAOD (440 nm) described in Sections 5.

The AOD map in Fig. 17 clearly shows a localized BB plume collocated with the one observed in the RGB image. More information about the aerosol event one can derive analyzing other retrieved extended optical properties. In particular, the maps for AE, ΔSSA, SSA and AAOD clearly show the changes in aerosol chemical and physical properties (for example, the size and absorption) while it is being transported away from the source located in Spain.

First of all, it is well seen that near the Spain coast AE is very high, SSA is small with strong spectral dependence between 440 and 670 nm bands: AE(440–670) ~ 2, ΔSSA(440–670) ~ 0.1, SSA(440) ~ 0.87, and AAOD(440) ~ 0.2. Further away from the biomass burning origin these parameters change essentially: AE < ~1.8, ΔSSA ~0.05, SSA ~0.9–0.95, and AAOD < ~0.1. Such behavior of the extended optical characteristics shows that further from the Spain coast (further from BB origin) the transported BB aerosol particles become bigger and less absorbing.

As one can see in Fig. 17, AE, SSA and ΔSSA are quite similar over essential part of the Mediterranean region both inside and outside of the observed plume of AOD. In other words, extended aerosol

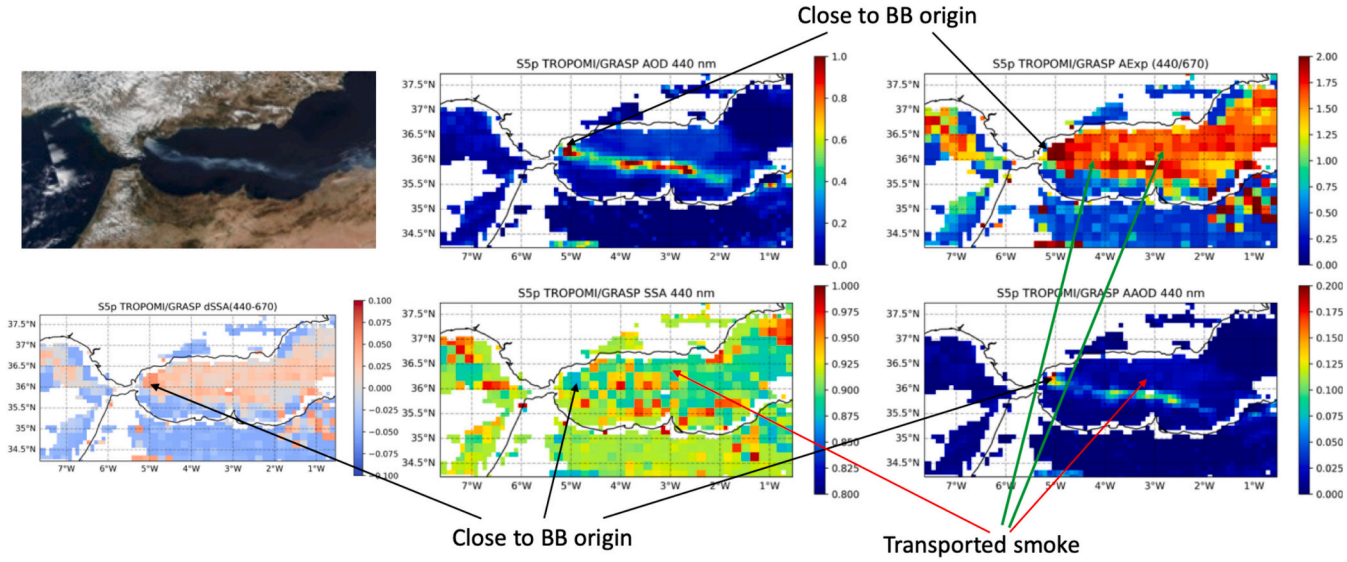

Fig. 17. Biomass Burning plume over Mediterranean region. September 9, 2021.

characteristics in Fig.17 clearly show that BB smoke is transported all over the Mediterranean Sea affecting air quality of the entire region. In this regard, extended aerosol properties provide crucial information which allow identifying aerosol sources and monitoring aerosol transport.

Another example of BB retrieval over Siberia is presented in Fig. 18. Similarly, to Fig. 17, the smoke from biomass burning can be identified using AE, ΔSSA, SSA, AAOD and other extended aerosol parameters. In particular, over the entire region AE is very high (bigger than 1.5) which corresponds to small particles. Absorption properties of smoke for this event varies essentially over the region: one can observe absorbing small particles localized over small areas (with AE > ~1.5, ΔSSA> ~0.05 and SSA(440) < ~0.95), as well as less absorbing smoke (SSA > ~0.95) with smaller spectral dependence (ΔSSA ~0.05–0) distributed over vast area in Siberia with quite similar AE > ~1.5.

The retrieved extended parameters properties (AE, ΔSSA, SSA, AAOD etc.) of the biomass burning smoke are quite different in their absorption properties for the Mediterranean and Siberia regions in Figs. 17 and 18. In general, the retrieval shows more absorbing BB aerosol over Mediterranean than over Siberia. This is due to the fact that the chemical, physical and morphological properties of smoke particles depend strongly on initial conditions (for example, type of organic matter being burnt (wood, vegetation etc.), the temperature of the fire, the wind and humidity conditions etc.). Therefore, different conditions over the Mediterranean and Siberia regions result in different optical properties of the BB aerosol.

The increase of particle size and reduced absorption of transported aerosol, observed in both Figs. 17 and 18, corresponds well to the general understanding of the process of smoke particle ageing in the atmosphere: due to collisions, fluffy soot aggregates may transform to a more closely packed clusters of particles, which then can be coated with water, absorb it or may attach to other aerosol particles in atmosphere (Dubovik et al. 2002; Reid et al., 2005; Adachi et al., 2010; Chen et al., 2010).

Fig. 19 shows another example of TROPOMI/GRASP retrieval over India, Nepal, Pakistan and Bangladesh region on November 27, 2019. From AOD retrieval, one can observe strong aerosol pollution in North and West (Pakistan) parts of the Indian Subcontinent (AOD (440 nm) >

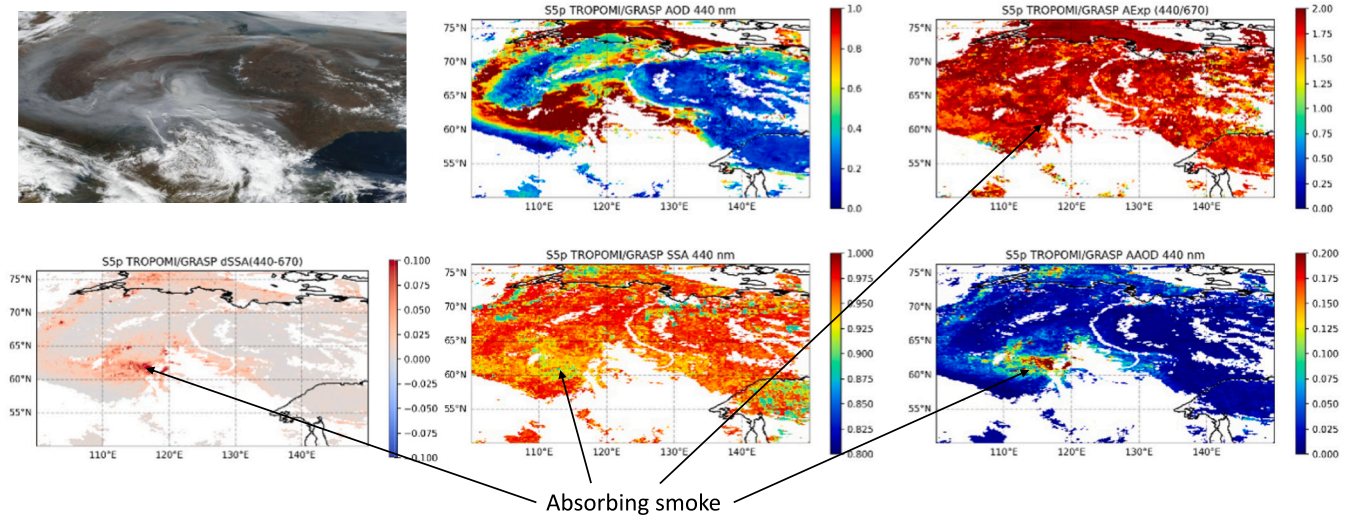

Fig. 18. Biomass Burning smoke over Siberia, September 25, 2020.

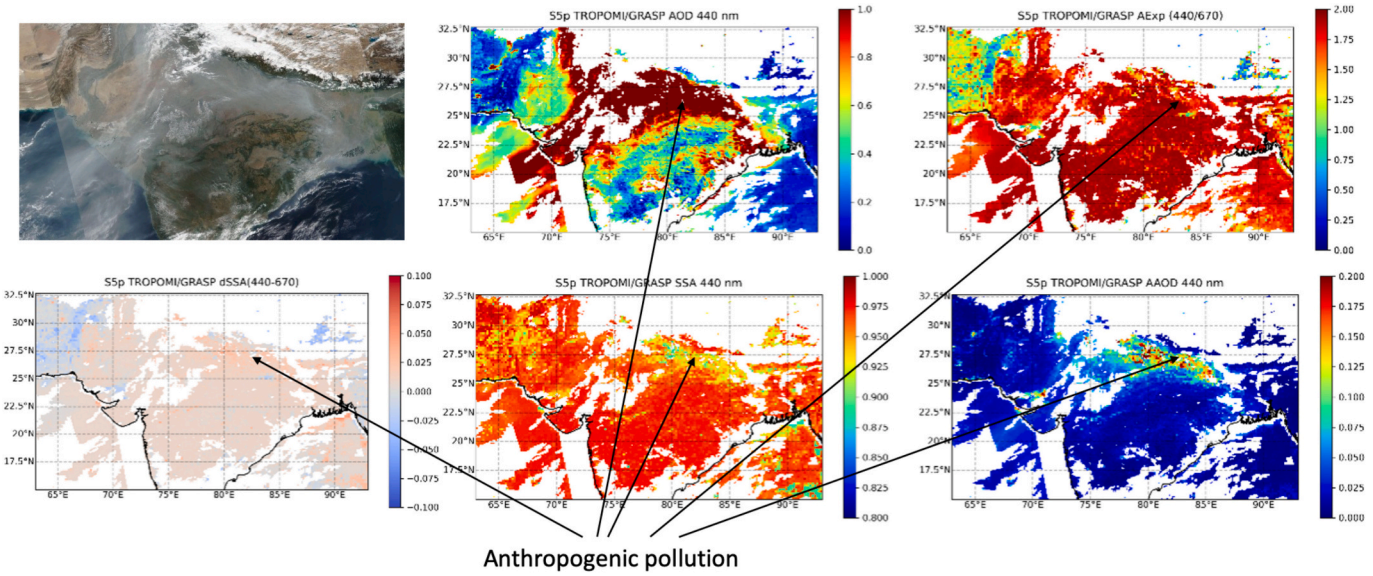

Fig. 19. Anthropogenic pollution over the Indian Subcontinent, November 27, 2019.

1). The central and South regions of India are less polluted on November 27, 2019 with moderate values of AOD (440 nm) about 0.3 – 0.8. Analyzing the aerosol pollution using the same extended characteristics as in Figs. 17 and 18, one can observe some similarities but also essential differences between BB smoke in Figs. 17, 18 and aerosol in Fig. 19. In particular, according to the retrieval results, aerosol over North part of Indian Subcontinent are very absorbing small particles with SSA (440 nm) value about 0.87 – 0.95, ΔSSA (440–670) ~0.02, AE > ~1.5–1.8, and AAOD (440 nm) > ~0.1, which, at first sight, correspond to the general description of absorbing BB smoke in Figs. 17 and 18. At the same time, considering SSA, AE, and ΔSSA parameters jointly, one can observe different behavior in Fig. 19 than in Figs.17 and 18 representing BB smoke. Firstly, the area on the North part of the Indian Subcontinent in Fig. 19 demonstrates low value of SSA (about 0.87–0.95) but with smaller AE (about 1.5–1.8) than for absorbing smoke over the Mediterranean region. Secondly, absorbing fine aerosol particles in Fig. 19 have essentially smaller spectral dependence of SSA than for absorbing smoke both over the Mediterranean and Siberia regions: AE ~1.5–1.8, SSA ~0.87–0.95, ΔSSA(440–670) < ~ 0.02 in Fig. 19 versus AE ~1.5–2, SSA ~0.87–0.95, ΔSSA(440–670) > ~ 0.05 in Figs. 17 and 18. Thirdly, over Central and South part of the Indian Subcontinent fine slightly absorbing particles (with SSA (440 nm) > ~0.97 and negligible SSA spectral dependence between 440 and 670 nm (ΔSSA(440–670) ~ 0)) are a little bit smaller than the slightly absorbing fine particles in Figs. 17 and 18: AE > ~1.8 vs AE > ~1.5, respectively.

These observations from the joint AE, SSA, and ΔSSA analysis indicates the presence of absorbing or non-absorbing aerosol particles over the Indian Subcontinent whose spectral dependence and size differ from what is typical for BB smoke aerosol. The aerosol event in Fig. 19 is rather related to the anthropogenic pollution which is often observed over India.

It was noted in Section 5.3 that the retrieved AE in TROPOMI/GRASP product is overestimated for big particles. Despite this fact, the joint analysis of the TROPOMI/GRASP extended aerosol properties allows identifying coarse components of aerosol, for example, dust. Fig. 20 presents the results of TROPOMI/GRASP inversion over North Africa on December 19, 2019. Several areas are selected in the figure covering major aerosol events according to the TROPOMI/GRASP AOD retrieval.

Taken into considerations only pixels with AOD (440 nm) values higher than 0.4, one can find the following extended parameters for areas 1 and 2: AE values between ~0.2 and 0.7 (big particles), SSA (440 nm) ~ 0.93 – 0.95 (essential absorption at short wavelengths) and ΔSSA

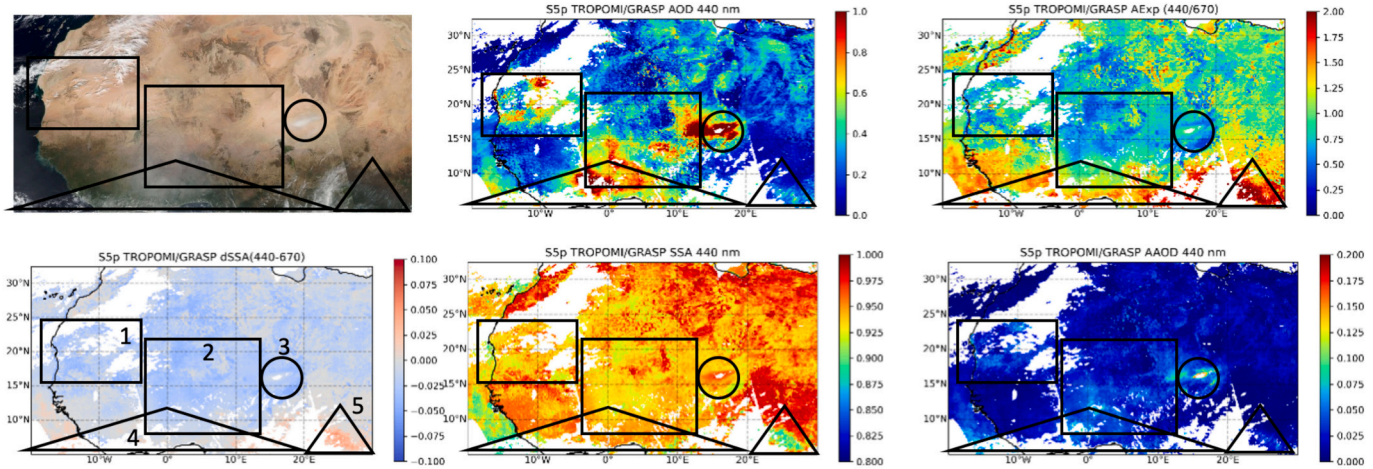

Fig. 20. Emitted and transported aerosol over the Sahara, December 19, 2019.

(440–670) < −0.02 (essential decreasing of absorption for longer wavelengths). Such parameters are typical for aerosol with domination of Saharan desert dust.

The pixels for the area 3 in Fig. 20, which correspond to high AOD event, show essentially different extended properties than for the areas 1 and 2. Here, one can see higher AE values from 0.7 to 1 (smaller coarse particles), much less absorbing aerosol with SSA(443) ~ 0.95 − 0.97 and smaller spectral dependence of SSA between blue and red bands (ΔSSA(440–670) ~ −0.02) than for areas 1 and 2. Geographically, the high AOD event in Fig. 20 is collocated with the Bodélé Depression area, which is a well-known as the biggest source of dust emission (Koren and Kaufman, 2004; Washington and Todd, 2005). It is located at dried out part of Lake of Chad with surface consist of quartz, silt, as well as sediments like fossilized diatoms forming a layer of fine dust of white color (see RGB image in Fig. 20). The physical and chemical properties of Bodélé Depression surface are quite different from those for the areas 1 and 2. This explains the differences in the retrieved properties of the wind-blown dust, showing presence of smaller and less absorbing dust particles over the Bodélé Depression than over the West and Central Sahara regions.

The higher AE and SSA values (smaller and less absorbing in 440 nm coarse particles) for dust over the Bodélé Depression than for the dust originated from West part of Sahara can be observed also from PARASOL/GRASP retrieval. In particular, Fig. 21 shows AE from PARASOL/GRASP is about 0.5–0.7 over Bodélé Depression which indicates the presence of smaller dust particles than over majority of other regions in Sahara dessert.

Due to multi-angular polarimetric measurements, the information content of PARASOL/POLDER instrument is sufficient for very high-quality retrieval of AE (Chen et al., 2020). In this regard, the observed consistent dust retrieval from the PARASOL/POLDER and S5P/TROPOMI observations can serve as indirect verification of the TROPOMI/GRASP product over areas like the Bodélé Depression which are stable aerosol sources for long period of time.

As shown in Section 5.3, TROPOMI/GRASP AE value (and logically AODF/AOD ratio) for coarse particles is overestimated. This is well seen in Figs. 20 and 21 for Saharan dust. In particular, AE from the TROPOMI/GRASP product is 0.3–0.5 higher than from the PARASOL/GRASP (Figs. 20 and 21), which corresponds to positive bias of AE value for coarse particles estimated from the validation with AERONET (Fig. 8). Nevertheless, even overestimated AE and AODF/AOD ratio allow clear discrimination between fine and coarse aerosol modes as seen in Figs. 17–20. As it was discussed in Section 5.3, the existing slopes in current TROPOMI retrievals can be corrected with more elaborated aerosol models with a more reliable spectral dependence and size distribution.

Some overestimations of the retrieved AE over the Sahara in TROPOMI/GRASP can be explained also by mixing dust and biomass burning. This mixing is well seen for the overlapping region of the areas 2 and 4 in Fig. 20 where one can observe extended characteristics typical for the mixture of BB and dust aerosols: AE ~ 1–1.5, SSA (440 nm) ~ 0.92–0.95 and ΔSSA (440–670) ~ −0.02 - 0.

The presence of BB smoke is well seen in the nonoverlapping part of the area 4 as well as in the area 5 in Fig. 20. With its extended properties BB smoke in the area 4 corresponds well to the transported and less absorbing BB smoke in the Siberia region (Fig. 18), while over area 5 it corresponds to absorbing smoke (SSA (440) ~ 0.87–0.9) consisting of very small particles (AE ~ 2) with essential spectral dependence of SSA from 440 to 670 nm (ΔSSA(440–670) > ~0.03) (Figs.17, 18 and 20).

The summary of extended aerosol properties considered for several aerosol events is presented in Table 8. In addition to AE parameter the ratio of fine and total AOD at 440 nm (AODF (440 nm)/AOD (440 nm)) calculated from the TROPOMI/GRASP product is also presented. This ratio correlates with AE but allows better understanding of contribution of fine and coarse mode to the optical characteristics.

Table 8 presents a preliminary analysis showing the possibilities of characterization of different aerosol species using extended retrieval properties from the TROPOMI/GRASP product. Detailed global analysis for different aerosol events with statistical distribution for each parameter is the subject of future studies, in particular, based on the PARASOL and TROPOMI retrievals with GRASP algorithm.

7. Conclusions

Analysis of aerosol and surface properties retrieved with GRASP showed a rich information content of S5P/TROPOMI for aerosol and surface characterization. With properly adapted forward models and the numerical inversion approaches GRASP multi-pixel retrieval of S5P/TROPOMI measurements allows extended aerosol and surface characterization, which is thought to be possible mainly from multi-angular/polarimetric measurements.

In addition to the traditional spectral AOD characteristic, TROPOMI/GRASP retrieval provides aerosol absorbing properties, represented by spectral Single Scattering Albedo (SSA) and spectral Absorbing AOD (AAOD), particles size represented by Angstrom Exponent (AE) parameter, fine mode AOD (AODF) etc. For each aerosol characteristic the Quality Assurance Index (QA and QAExtend) is associated, and recommendation of their usage are provided in the paper, allowing selecting

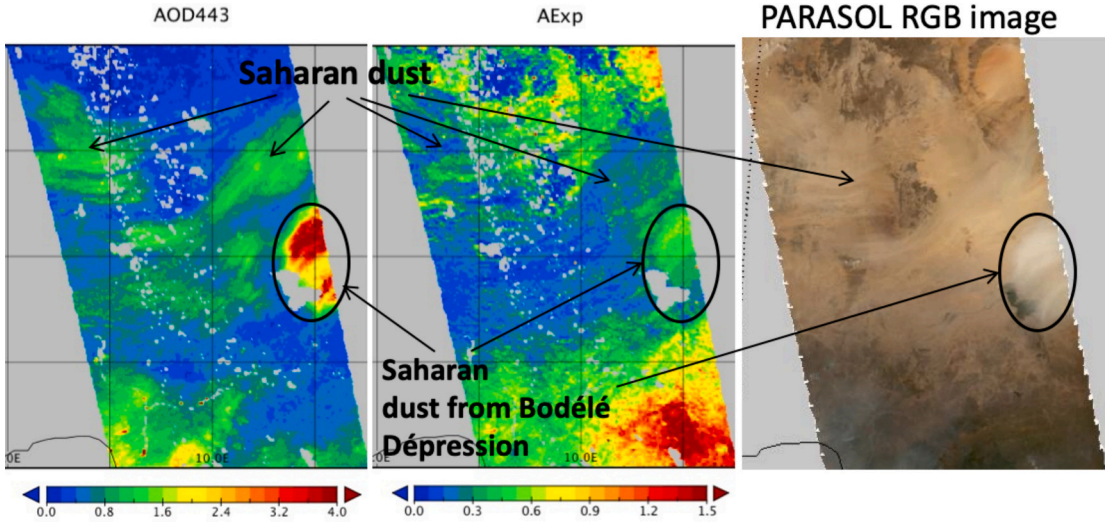

Fig. 21. Aerosol properties from PARASOL/GRASP over Sahara, February 18, 2018.

Table 8
Extended aerosol characteristics for several aerosol events.

Aerosol Extended Properties	Mediterranean BB		Siberian BB		Anthropogenic aerosol over Indian Subcontinent		Saharan dust	
	Absorbing Smoke	Less Absorbing Smoke	Absorbing Smoke	Less Absorbing Smoke	North Part	Central and South Part	West and Central Sahara	Bodélé Depression
Angstrom Exponent AE(440–670)	> ~ 2	~1.5–1.7	> ~1.5	> ~1.5	~1.5–1.8	> ~ 1.8	~0.2–0.7	~0.7–1
SSA(440)	~0.87	~ 0.9–0.95	~ 0.9–0.95	> ~0.95	~ 0.87–0.95	> ~ 0.97	~ 0.93–0.95	~ 0.95–0.97
ΔSSA(440–670)	> ~0.07	~ 0–0.07	> ~ 0.05	~ 0–0.05	~ 0.02	~ 0–0.02	~ −0.03	~ −0.02 - 0
$\frac{AODF(440)}{AOD(440)}$	~1	~ 0.8–0.9	~ 0.8–1	~ 0.8–1	~ 0.8–0.9	> ~ 0.9	~ 0.3–0.5	~ 0.5–0.7

the best retrieval results according to requirements of studies.

Overall, the results of validation versus AERONET of all optical characteristics (AOD, SSA, AAOD, ΔSSA and AE) obtained from S5P/TROPOMI demonstrate high quality and fulfilment of "optimized" GCOS-based requirements for aerosol characterization from space-borne measurements. The analyses performed over different areas show sensitivity of the retrieved extended properties to different aerosol type including biomass burning, anthropogenic pollution and dust events. Since the end of the PARASOL mission in 2013, there are no global reliable satellite SSA products covering wide spectral ranges. There is also a lack of reliable satellite AE products which are related to the size of aerosol. These and other extended aerosol characteristics are becoming more and more demanded in aerosol and climate studies. In this regard, despite identified shortcomings, extended aerosol characterization from S5P/TROPOMI provided by GRASP is expected to fill a gap in the aerosol satellite products.

Results of global intercomparison of surface products also showed good correspondence of TROPOMI/GRASP BRDF and derived surface albedos with GROSAT and MODIS surface datasets for the overlapping spectral channels. TROPOMI/GRASP full BRDF parameters were derived independently of any a priori knowledge i.e., without relying on existing surface climatology. The selected spectral bands from UV, VIS, NIR and SWIR ranges allow proper interpolating and extrapolating of the surface properties to other bands required for aerosol, trace gases and clouds studies.

Though the validation with AERONET and surface reference datasets showed rather high reliability of TROPOMI/GRASP product with high percentage of fulfilment of the formulated requirements, some limitations of current TROPOMI/GRASP products are identified and described in this paper. In particular, the retrieval shows about 0.3 overestimation in AE (440–670) values for coarse aerosol (TROPOMI/GRASP retrieves smaller particles for coarse aerosol mode). Further improvement of the retrieval can be done with more correct spectral dependence (from UV to SWIR) and size distribution in the aerosol models.

In general, the studies based on the S5P/TROPOMI retrieval with GRASP algorithm demonstrate that accurate extended aerosol and surface characterization can be achieved from single viewing instruments when several main conditions are fulfilled simultaneously. Firstly, the instrument should measure in the wide spectral range (for example, in UV, VIR, NIR and SWIR like S5P/TROPOMI) providing rich spectral information about aerosol and surface. Secondly, the swath of measurements should be big enough for frequent overpassing over the same ground pixel (at least several times per week, but preferably daily or more frequent revisiting time). This requirement is crucial for retrievals from single viewing instruments allowing to account (i) for the different temporal variability of aerosol and surface properties and (ii) for angular dependence of surface reflectance to retrieve BRDF model parameters. Thirdly, algorithms applied to such retrieval measurements should be able to treat multi-temporal information. These measurement and algorithmic requirements can be complimented by others, for example, by properly physically constrained forward aerosol and surface models as discussed in this paper.

CRediT authorship contribution statement

Pavel Litvinov: Writing – review & editing, Writing – original draft, Supervision, Investigation, Conceptualization. **Cheng Chen:** Writing – review & editing, Writing – original draft, Visualization, Validation, Investigation. **Oleg Dubovik:** Writing – review & editing, Investigation, Formal analysis. **Lukas Bindreiter:** Software, Data curation. **David Fuertes:** Resources, Formal analysis, Data curation. **Anton Lopatin:** Validation, Formal analysis. **Tatyana Lapyonok:** Software, Formal analysis. **Verena Lanzinger:** Software, Formal analysis. **Andreas Hangler:** Software, Data curation. **Michael Aspetsberger:** Software, Data curation. **Martin de Graaf:** Writing – review & editing, Investigation, Formal analysis. **Lieuwe Gijsbert Tilstra:** Writing – review & editing, Investigation, Formal analysis. **Piet Stammes:** Writing – review & editing, Investigation. **Alexandru Dandocsi:** Writing – review & editing, Formal analysis. **Daniele Gasbarra:** Writing – review & editing, Formal analysis. **Elody Fluck:** Writing – review & editing, Formal analysis. **Claus Zehner:** Writing – review & editing, Formal analysis. **Christian Retscher:** Writing – review & editing, Project administration.

Declaration of competing interest

The authors declare that they have no known competing financial interests or personal relationships that could have appeared to influence the work reported in this paper.

Data availability

The Sentinel-5P/TROPOMI GRASP aerosol and surface products are publicly available at GRASP-OPEN website (https://www.grasp-open.com/products/tropomi-data-release/)

Acknowledgments

The studies presented in this paper were performed in the framework of ESA (European Space Agency) S5P + Innovation program, Theme 5: AOD + BRD (ESA. Contract No. 4000127614/19/I-NS).

(https://eo4society.esa.int/projects/sentinel-5p-innovation-aod-brdf/). Authors would like to gratefully acknowledge AERONET network for freely available data used for validation purposes in this studies. The retrieval results presented in this paper were obtained with GRASP-OPEN software (https://www.grasp-open.com) and are available at GRASP-OPEN web site (https://www.grasp-open.com/products/tropomi-data-release/).

Appendix A. Single and multi-pixel constraints in TROPOMI/GRASP retrieval

GRASP inversion approach realizes the statistically optimized retrieval based on Multi-Term Least Square Method (LSM) and applies in the unified way different a priori constraints on the initial guess of the retrieved parameters, "single-" and "multi-pixel" smoothness (Dubovik and King, 2000, Dubovik 2004, Dubovik et al., 2011, 2014, 2021b). The smoothness constraints limit the spectral, shape, spatial and temporal variability of the retrieved parameters by applying limitations on their first, second and other orders of derivatives (Dubovik et al., 2011, 2021a). The terms "single-pixel" and "multi-pixel" constraints are related to the case when the retrieval is conducted for satellite measurements over one selected pixel or for a group of several pixels simultaneously. Correspondingly, the "single-pixel" approach applies the constraints on the parameters for each pixel independently, and the "multi-pixel" approach constrains the spatial or temporal variability of the retrieved parameters between different pixels (Dubovik et al., 2011, 2021b). For the forward models chosen in the TROPOMI/GRASP retrieval, the "single-pixel" smoothness constraints limit the spectral dependence of wavelength dependent parameters (for example, first BRDF parameter) and aerosol model weights (fractions) dependencies.

GRASP applications to different satellites demonstrated the crucial role of the smoothness constraints for stable and accurate characterization of both atmospheric aerosol and Earth's surface (Dubovik et al., 2011, 2014, 2021b; Chen et al., 2022b). In the framework of the ESA S5P + I AOD/BRDF project (TROPOMI, 2022b), extensive tests for evaluating the efficiency of different a priori constrains were performed to identify the most optimal GRASP retrieval approach for the S5P/TROPOMI instrument.

Table A1 contains a brief description of the applied constraints for the TROPOMI/GRASP retrieval over land and sea/ocean surfaces.

Table A1
GRASP smoothness constraints adapted for TROPOMI measurements.

	Retrieved parameter	Constraints	Order of Derivative (Smoothness order)	Lagrange multiplier
1	Relative fractions for each aerosol component c_k ($k = 1.0.4$)	*Multi-pixel spatial smoothness*	1	0.1
		Multi- pixel temporal smoothness	1	0.01
2	Total column volume concentration c_v	*Multi-pixel spatial smoothness*	1	0
		Multi-pixel temporal smoothness	1	0
3	Aerosol height scale parameter	*Multi-pixel spatial smoothness*	1	0.1
		Multi-pixel temporal smoothness	1	0.001
4	Isotropic BRDF parameter	Single pixel spectral smoothness	1	0.001
	(retrieval over land)	*Multi-pixel spatial smoothness*	1	0
		Multi-pixel temporal smoothness	1	1
5	Volumetric BRDF parameter	*Multi-pixel spatial smoothness*	1	0
	(retrieval over land)	Multi-pixel temporal smoothness	1	1
6	Geometric BRDF parameter	*Multi-pixel spatial smoothness*	1	0
	(retrieval over land)	Multi- pixel temporal smoothness	1	1
7	Water body reflectance	Single pixel spectral smoothness	1	10^{-8}
	(retrieval over sea/ocean)	*Multi-pixel spatial smoothness*	1	0.001
		Multi-pixel temporal smoothness	1	5
8	Foam free water surface fraction	*A priory initial guess*	–	10
	(retrieval over sea/ocean)	*Multi-pixel spatial smoothness*	1	0.1
		Multi-pixel temporal smoothness	–	–
9	Mean square water surface slope	*A priory initial guess*	–	10
	(retrieval over sea/ocean)	*Multi-pixel spatial smoothness*	1	0.1
		Multi-pixel temporal smoothness	–	–

As mentioned in Section 4.1.1, the retrieval parameters of GRASP "aerosol models" approach, which are used for TROPOMI/GRASP retrieval, are spectrally independent (Eqs. (1)–(4)). Moreover, being represented in the form given by Eqs. (7)–(17), BRDF model used for TROPOMI/GRASP processing has only one spectrally dependent parameter. Therefore, the spectral smoothness constraints are applied only on the spectrally dependent first BRDF parameter $a_{iso}(\lambda)$ for land and $r_{WhC}(\lambda)$ for water surfaces (Eqs. (7)–(17)). The detailed description of the smoothness constraints in the GRASP algorithm can be found in (Dubovik et al., 2021a).

Appendix B. TROPOMI/GRASP product quality specification

Aerosol and surface characteristics retrieved from space-borne remote sensing are always affected by such artifacts as non-accounted cloud contamination or cloud shadows, errors in data measurements or data regridding, complex structure of underling surface reflection due to surface topology (mountain and coastal areas, land and water mixed surfaces etc.) where the applied BRDF model does not work etc. This results in non-convergence of the retrieval or outliers in the retrieved atmosphere and surface parameters. Therefore, an essential part of the satellite retrieval product preparation is always related to proper evaluation of data quality.

The detailed description of data quality assurance procedure applied to TROPOMI/GRASP aerosol and surface product is presented in (TROPOMI ATBD of GRASP AOD + BRDF, 2021; TROPOMI, 2022b). It consists of several sequential post-processing tests performed on the retrieved datasets: 1. "Residual" test; 2. Moving 3 × 3 window "Standard Deviation AOD" test; 3. Static 5 × 5 window QA test; 4. Quality assignment to advanced aerosol properties.

The fitting "residuals" test is applied at each pixel. It provides basic data filtering corresponding to non-converged inversion cases with the value of relative and absolute fitting residuals higher than specified thresholds which are different for water and land pixels. Moreover, the thresholds for land pixels depends on the surface types and are defined for four different NDVI ranges: (i) NDVI <0.1 (bare soil mainly); (ii) $0.1 \leq$NDVI <0.4 (mixture of soil and vegetation); (iii) $0.4 \leq$NDVI <0.6 (vegetation); (iv) NDVI ≥ 0.6 (dense vegetation). Over water and very bright bare land surfaces (NDVI <0.1 and White Sky Albedo at 670 nm bigger than 0.3) the thresholds are further defined according to AOD (670 nm) values: separately for AOD(670) < 1 and AOD(670) ≥ 1 (TROPOMI ATBD of GRASP AOD + BRDF, 2021).

To all pixels which passed the "residual" test the value of Quality Assurance (QA) index is assigned to 1. At the next two steps ("Standard Deviation AOD" and "Static QA" tests) QA value can change to the value 2 or 3 representing "good" and "very good" quality of retrieval.

The basic idea of the second "Standard Deviation AOD" test is based on the analysis of both absolute and relative values of standard deviation of AOD obtained for pixels within a 3 × 3 moving window. The pixels with absolute standard deviation <0.1 or relative standard deviation <15% are assigned to QA value 2 (good quality). The pixels with absolute standard deviation <0.05 or relative standard deviation <15% are assigned to QA value 3 (very good quality). Strictly speaking, the QA value assignment in this second test also depends on the value of the relative residual and the total number of pixels in the 3 × 3 moving window, which may change the distribution of pixels among "good" and "very good" quality assurance categories. A detailed diagram with flowchart logic for "Standard Deviation AOD" is available in the GRASP/TROPOMI ATBD (TROPOMI ATBD of GRASP AOD + BRDF, 2021).

The "static QA" test counts for statistic of pixels with different QA values within a static 5 × 5 pixels window. Depending on the dominated category, QA value for pixels within the window can change from 3 back to 2 and from 2 to 1 (from "very good" to "good" and from "good" to "marginal" category) (TROPOMI ATBD of GRASP AOD + BRDF, 2021).

When QA values are assigned, the additional quality assurance test is applied for such advanced retrieved aerosol properties as: Angstrom Exponent (AE), Single Scattering Albedo (SSA) and aerosol model fractions (relative concentrations). The reason for this additional test is well-known and related to the reduced sensitivity to the microphysical aerosol properties (size, complex refractive index, non-sphericity etc.) at low AOD values. In particular, the AERONET L2 inversion product provides data only for the case when AOD(440 nm) is higher than 0.4 (Dubovik et al., 2000). For extended aerosol parameters of TROPOMI/GRASP product we apply a similar threshold but different over land and water surfaces. In particular, QA index value for all advanced aerosol properties (QAExtend in GRASP/TROPOMI product) is set up to 1 ("marginal" category) if AOD(670) < 0.1 over land and AOD(670) < 0.05 over ocean indicating poor expectation in the retrieval quality of the advanced properties at low aerosol loading values. Maximum values of AOD(670) threshold which define the best expected retrieval quality of the advanced aerosol characteristics is chosen to be 0.3 over land and 0.2 over water. These maximum thresholds are quite subjective and chosen to keep balance between the sufficient number of pixels in "very good" category both over land and ocean on one hand and reasonable quality of advanced properties in this category on another hand (TROPOMI ATBD of GRASP AOD + BRDF, 2021). For all pixels with AOD(670) bigger than 0.3 (land) and 0.2 (water) the quality index "QAExtend" for advanced properties is taken exactly the same value as QA from previous three tests. For 0.1 < AOD(670) < 0.3 (land) and 0.05 < AOD(670) < 0.2 (water) it takes the same value as QA if QA = 1 or QA = 2 and is equal 2 if QA = 3.

The example of the global distribution of pixel level quality assurance (QA) index occurrence is presented in Fig. 6. As one can see, most of the pixels are assigned to "good" (QA≥2) and "very good" (QA≥3) categories. The pixels with "marginal" (QA≥1) retrieval quality are mainly distributed over bright surfaces like Sahara and Atacama desert, Arabic semi-island or over mountain areas. The validation of retrieved aerosol properties for each quality assurance category is discussed in the section 5.

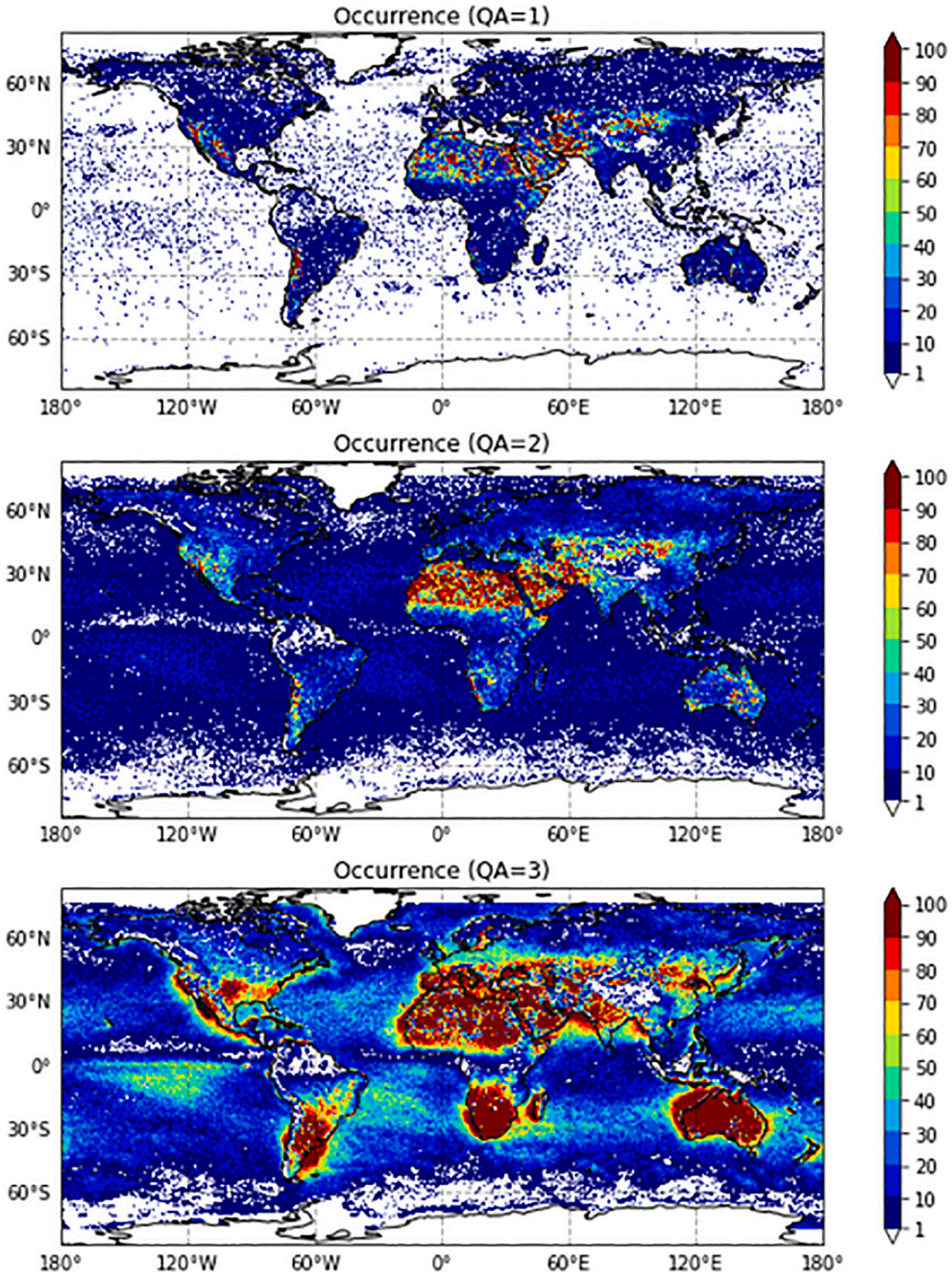

Fig. A1. Global distribution of the pixel level occurrence of the Quality Assurence (QA) index: QA = 1, QA = 2 and QA = 3 from March 2019 till February 2020.

References

Adachi, K., Chung, S.H., Buseck, P.R., 2010. Shapes of soot aerosol particles and implications for their effects on climate. J. Geoph. Res. 115, D15206 https://doi.org/10.1029/2009JD012868.

Bohren, C.F., Huffman, D.R., 1998. Absorption and Scattering of Light by Small Particles. Wiley, NewYork.

Bovensmann, H., Burrows, J.P., Buchwitz, M., Frerick, J., Noël, S., Rozanov, V.V., et al., 1999. SCIAMACHY: Mission objectives and measurement modes. J. Atmos. Sci. 56 (2), 127–150. https://doi.org/10.1175/1520-0469(1999)056<0127:SMOAMM>2.0.CO;2.

Burrows, J.P., Hölzle, E., Goede, A.P.H., Visser, H., Fricke, W., 1995. SCIAMACHY—scanning imaging absorption spectrometer for atmospheric chartography. Acta Astronaut. 35 (7), 445–451. https://doi.org/10.1016/0094-5765(94)00278-T.

Cao, C., Xiong, J., Blonski, S., Liu, Q., Uprety, S., Shao, X., et al., 2013. Suomi NPP VIIRS sensor data record verification, validation, and long-term performance monitoring. J. Geophys. Res. Atmos. 118 (20), 11,664–11,678. https://doi.org/10.1002/2013JD020418.

Chen, L.-W.A., Verburg, P., Shackelford, A., Zhu, D., Susfalk, R., Chow, J.C., Watson, J. G., 2010. Moisture effects on carbon and nitrogen emission from burning of wildland biomass. Atmos. Chem. Phys. 10, 6617–6625. https://doi.org/10.5194/acp- 10-6617-2010.

Chen, C., Dubovik, O., Henze, D.K., Chin, M., Lapyonok, T., Schuster, G.L., et al., 2019. Constraining global aerosol emissions using POLDER/PARASOL satellite remote sensing observations. Atmospheric Chemistry and Physics 19 (23), 14585–14606. https://doi.org/10.5194/acp-19-14585-2019.

Chen, C., Dubovik, O., Fuertes, D., Litvinov, P., Lapyonok, T., Lopatin, A., et al., 2020. Validation of GRASP algorithm product from POLDER/PARASOL data and assessment of multi-angular polarimetry potential for aerosol monitoring. Earth System Science Data 12 (4), 3573–3620. https://doi.org/10.5194/essd-12-3573-2020.

Chen, C., Dubovik, O., Schuster, G.L., Chin, M., Henze, D.K., Lapyonok, T., Li, Z., Derimian, Y., Zhang, Y., 2022a. Multi-angular polarimetric remote sensing to pinpoint global aerosol absorption and direct radiative forcing. Nat. Commun. 13 (1), 7459.

Chen, C., Dubovik, O., Litvinov, P., Fuertes, D., Lopatin, A., Lapyonok, T., et al., 2022b. Remote Sensing of Environment Properties of aerosol and surface derived from OLCI / Sentinel-3A using GRASP approach : Retrieval development and preliminary validation. Remote Sens. Environ. 280 (June), 113142. https://doi.org/10.1016/j.rse.2022.113142.

Chen, C., Litvinov, P., Dubovik, O., et al., 2024. Extended Aerosol and Surface Characterization from S5P/TROPOMI with GRASP Algorithm. Part II: Global Validation and Intercomparison. Remote Sens. Environ (submitted).

Choi, M., Kim, J., Lee, J., Kim, M., Park, Y.-J., Jeong, U., et al., 2016. GOCI Yonsei aerosol retrieval (YAER) algorithm and validation during the DRAGON-NE Asia 2012 campaign. Atmos. Meas. Tech. 9 (3), 1377–1398.

Climate Modelling User Group (CMUG), 2015. User Requirement Document, version 0.6. http://ensembleseu.metoffice.com/cmug/CMUG_PHASE_2_D1.1_Requirements_v0.6.pdf.

Cox, C., Munk, W., 1954. Measurement of the roughness of the sea surface from photographs of the Sun's glitter. J. Opt. Soc. Am. 44 (11), 838. https://doi.org/10.1364/josa.44.000838.

de Araujo Barbosa, C.C., Atkinson, P.M., Dearing, J.A., 2015. Remote sensing of ecosystem services: a systematic review. Ecol. Indic. 52, 430–443. https://doi.org/10.1016/J.ECOLIND.2015.01.007.

de Leeuw, G., Holzer-Popp, T., Bevan, S., Davies, W.H., Descloitres, J., Grainger, R.G., et al., 2015. Evaluation of seven European aerosol optical depth retrieval algorithms for climate analysis. Remote Sens. Environ. 162, 295–315. https://doi.org/10.1016/j.rse.2013.04.023.

Deschamps, P.-Y., Breon, F.-M., Leroy, M., Podaire, A., Bricaud, A., Buriez, J.-C., Seze, G., 1994. The POLDER mission: instrument characteristics and scientific objectives. IEEE Trans. Geosci. Remote Sens. 32 (3), 598–615. https://doi.org/10.1109/36.297978.

Dubovik, O., King, M.D., 2000. A flexible inversion algorithm for retrieval of aerosol optical properties from Sun and sky radiance measurements. J. Geophys. Res. Atmos. 105 (D16), 20673–20696. https://doi.org/10.1029/2000JD900282.

Dubovik, O., Smirnov, A., Holben, B.N., King, M.D., Kaufman, Y.J., Eck, T.F., Slutsker, I., 2000. Accuracy assessments of aerosol optical properties retrieved from aerosol robotic network (AERONET) Sun and sky radiance measurements. J. Geophys. Res. Atmos. 105 (D8), 9791–9806. https://doi.org/10.1029/2000JD900040.

Dubovik, O., Holben, B.N., Eck, T.F., Smirnov, A., Kaufman, Y.J., King, M.D., Tanre, D., Slutsker, I., 2002. Variability of absorption and optical properties of key aerosol types observed in worldwide locations. J. Atm. Sc. 59, 590–608. https://doi.org/10.1175/1520-0469(2002)059<0590:VOAAOP>2.0.CO;2.

Dubovik, O., Lapyonok, T., Kaufman, Y.J., Chin, M., Ginoux, P., Kahn, R.A., Sinyuk, A., 2008. Retrieving global aerosol sources from satellites using inverse modeling. Atmos. Chem. Phys. 8 (2), 209–250. https://doi.org/10.5194/acp-8-209-2008.

Dubovik, O., Herman, M., Holdak, A., Lapyonok, T., Tanré, D., Deuzé, J.L., et al., 2011. Statistically optimized inversion algorithm for enhanced retrieval of aerosol properties from spectral multi-angle polarimetric satellite observations. Atmos. Meas. Tech. 4 (5), 975–1018. https://doi.org/10.5194/amt-4-975-2011.

Dubovik, O., Lapyonok, T., Litvinov, P., Herman, M., Fuertes, D., Ducos, F., et al., 2014. GRASP: a versatile algorithm for characterizing the atmosphere. SPIE Newsroom. https://doi.org/10.1117/2.1201408.005558.

Dubovik, O., Li, Z., Mishchenko, M.I., Tanré, D., Karol, Y., Bojkov, B., et al., 2019. Polarimetric remote sensing of atmospheric aerosols: instruments, methodologies, results, and perspectives. Journal of Quantitative Spectroscopy and Radiative Transfer 224, 474–511. https://doi.org/10.1016/J.JQSRT.2018.11.024.

Dubovik, O., Fuertes, D., Lytvynov, P., Lopatin, A., Lapyonok, T., Doubovik, I., et al., 2021a. A comprehensive description of multi-term LSM for applying multiple a priori constraints in problems of atmospheric remote sensing: GRASP algorithm, concept, and applications. Frontiers in Remote Sensing 1–23. https://doi.org/10.3389/FRSEN.2021.706851.

Dubovik, O., Schuster, G.L., Xu, F., Hu, Y., Bösch, H., Landgraf, J., Li, Z., 2021b. Grand Challenges in Satellite Remote Sensing. Frontiers in Remote Sensing 2 (February), 619818. https://doi.org/10.3389/frsen.2020.603650.

ESA Climate Change Initiative Aerosol_cci, 2019. User Requirement Document, version 4.3. http://cci.esa.int/sites/default/files/Aerosol_cci%2B_URD_v4.3_final.pdf.

Frouin, R., Pelletier, B., 2015. Bayesian methodology for inverting satellite ocean-color data. Remote Sens. Environ. 159, 332–360. https://doi.org/10.1016/J.RSE.2014.12.001.

Frouin, R., Schwindling, M., Deschamps, P.Y., 1996. Spectral reflectance of sea foam in the visible and near-infrared: in situ measurements and remote sensing implications. Journal of Geophysical Research C: Oceans 101 (C6), 14361–14371. https://doi.org/10.1029/96JC00629.

GCOS, 2016. The Global Observing System for Climate: Implementation Needs (GCOS200).

Giles, D.M., Sinyuk, A., Sorokin, M.G., Schafer, J.S., Smirnov, A., Slutsker, I., et al., 2019. Advancements in the aerosol robotic network (AERONET) version 3 database – automated near-real-time quality control algorithm with improved cloud screening for Sun photometer aerosol optical depth (AOD) measurements. Atmos. Meas. Tech. 12 (1), 169–209. https://doi.org/10.5194/amt-12-169-2019.

Govaerts, Y.M., Wagner, S., Lattanzio, A., Watts, P., 2010. Joint retrieval of surface reflectance and aerosol optical depth from MSG/SEVIRI observations with an optimal estimation approach: 1. Theory. Journal of Geophysical Research: Atmospheres 115 (D2).

Hasekamp, O.P., Landgraf, J., 2007. Retrieval of aerosol properties over land surfaces: capabilities of multiple-viewing-angle intensity and polarization measurements. Appl. Optics 46, 3332–3344. https://doi.org/10.1364/AO.46.003332.

Hasekamp, O.P., Litvinov, P., Butz, A., 2011. Aerosol properties over the ocean from PARASOL multiangle photopolarimetric measurements. J. Geophys. Res. 116 (D14204), 2011. https://doi.org/10.1029/2010JD015469.

Hasekamp, O., Litvinov, P., Fu, G., Chen, C., Dubovik, O., 2024. Algorithm evaluation for polarimetric remote sensing of atmospheric aerosols. Atmos. Meas. Tech. 17, 1497–1525.

Herman, M., Deuzé, J.L., Devaux, C., Goloub, P., Bréon, F.M., Tanré, D., 1999. Remote sensing of aerosols over land surfaces including polarization measurements and application to POLDER measurements. J. Geophys. Res. 102, 17039–17049. https://doi.org/10.1029/96JD02109.

Holben, B.N., Eck, T.F., Slutsker, I., Tanré, D., Buis, J.P., Setzer, A., et al., 1998. AERONET—A federated instrument network and data archive for aerosol characterization. Remote Sens. Environ. 66 (1), 1–16. https://doi.org/10.1016/S0034-4257(98)00031-5.

Hollmann, R., Merchant, C.J., Saunders, R., Downy, C., Buchwitz, M., Cazenave, A., et al., 2013. The ESA climate change initiative: satellite data Records for Essential Climate Variables. Bull. Am. Meteorol. Soc. 94 (10), 1541–1552. https://doi.org/10.1175/BAMS-D-11-00254.1.

Hsu, N.C., Jeong, M.-J., Bettenhausen, C., Sayer, A.M., Hansell, R., Seftor, C.S., et al., 2013. Enhanced deep blue aerosol retrieval algorithm: the second generation. J. Geophys. Res. Atmos. 118 (16), 9296–9315. https://doi.org/10.1002/jgrd.50712.

Hsu, N.C., Lee, J., Sayer, A.M., Kim, W., Bettenhausen, C., Tsay, S.-C., 2019. VIIRS deep blue aerosol products over land: extending the EOS long-term aerosol data records. J. Geophys. Res. Atmos. 124 (7), 4026–4053. https://doi.org/10.1029/2018JD029688.

IPCC, 2021. In: Masson-Delmotte, V., Zhai, P., Pirani, A., Connors, S.L., Péan, C., Berger, S., Caud, N., Chen, Y., Goldfarb, L., Gomis, M.I., Huang, M., Leitzell, K., Lonnoy, E., Matthews, J.B.R., Maycock, T.K., Waterfield, T., Yelekçi, O., Yu, R., Zhou, B. (Eds.), Climate Change 2021: The Physical Science Basis. Contribution of Working Group I to the Sixth Assessment Report of the Intergovernmental Panel on Climate Change, 2391. Cambridge University Press, Cambridge, United Kingdom and New York, NY, USA. https://doi.org/10.1017/9781009157896.

Kikuchi, M., Murakami, H., Suzuki, K., Nagao, T.M., Higurashi, A., 2018. Improved hourly estimates of aerosol optical thickness using spatiotemporal variability derived from Himawari-8 geostationary satellite. IEEE Trans. Geosci. Remote Sens. 56 (6), 3442–3455.

Kinne, S., Schulz, M., Textor, C., et al., 2006. An AeroCom initial assessment optical properties in aerosol component modules of global models. Atmos. Chem. Phys. 6, 1815–1834.

Kokhanovsky, A.A., 2013. 10. Earth Sci. Rev. 116 (1), 95–108. https://doi.org/10.1016/J.EARSCIREV.2012.10.008.

Koren, I., Kaufman, Y.J., 2004. Direct wind measurements of Saharan dust events from Terra and Aqua satellites. Geophysical Research Letters. American Geophysical Union. 31 (6).

Levelt, P.F., Hilsenrath, E., Leppelmeier, G.W., van den Oord, G.H.J., Bhartia, P.K., Tamminen, J., et al., 2006. Science objectives of the ozone monitoring instrument. IEEE Trans. Geosci. Remote Sens. 44 (5), 1199–1208. https://doi.org/10.1109/TGRS.2006.872336.

Levy, R.C., Mattoo, S., Munchak, L.A., Remer, L.A., Sayer, A.M., Patadia, F., Hsu, N.C., 2013. The collection 6 MODIS aerosol products over land and ocean. Atmos. Meas. Tech. 6 (11), 2989–3034. https://doi.org/10.5194/amt-6-2989-2013.

Li, X., Strahler, A.H., 1992. Geometric-optical bidirectional reflectance modeling of the discrete crown vegetation canopy: effect of crown shape and mutual shadowing. IEEE Trans. Geosci. Remote Sens. 30 (2), 276–292. https://doi.org/10.1109/36.134078.

Li, Z., Zhao, X., Kahn, R., Mishchenko, M., Remer, L., Lee, K.-H., et al., 2009. Uncertainties in satellite remote sensing of aerosols and impact on monitoring its long-term trend: a review and perspective. Ann. Geophys. 27 (7), 2755–2770. https://doi.org/10.5194/angeo-27-2755-2009.

Litvinov, P., Hasekamp, O., Cairns, B., Mishchenko, M., 2010. Reflection models for soil and vegetation surfaces from multiple-viewing angle photopolarimetric measurements. J. Quant. Spectrosc. Radiat. Transf. 111 (4), 529–539. https://doi.org/10.1016/j.jqsrt.2009.11.001.

Litvinov, P., Hasekamp, O., Cairns, B., 2011a. Models for surface reflection of radiance and polarized radiance: comparison with airborne multi-angle photopolarimetric measurements and implications for modeling top-of-atmosphere measurements. Remote Sens. Environ. 115 (2), 781–792. https://doi.org/10.1016/J.RSE.2010.11.005.

Litvinov, P., Hasekamp, O., Cairns, B., Mishchenko, M., 2011b. Semi-empirical BRDF and BPDF models applied to the problem of aerosol retrievals over land: testing on airborne data and implications for modeling of top-of-atmosphere measurements. In: Polarimetric Detection, Characterization and Remote Sensing. Springer, Dordrecht, pp. 313–340. https://doi.org/10.1007/978-94-007-1636-0_13.

Litvinov, P., Dubovik, O., Chen, C., et al., 2020. Combined Retrieval from Ground Based and Space-borne Measurements: New Possibilities for Surface Validation and Beyond. AGU, 1-17 December.

Litvinov, P., Chen, C., Dubovik, O., Matar, C., Bindreiter, L., et al., 2022. Synergetic retrieval from ground-based and satellites measurements: new possibilities for surface characterization and validation. In: GROSAT final report (FR). Source: GRASP; issue 1.0. 2022.

Lopatin, A., Dubovik, O., Fuertes, D., Stenchikov, G., Lapyonok, T., Veselovskii, I., et al., 2021. Synergy processing of diverse ground-based remote sensing and in situ data using GRASP algorithm: applications to radiometer, lidar and radiosonde

observations. Atmospheric Measurement Techniques 14, 2575–2614. https://doi.org/10.5194/amt-14-2575-2021.
Ludewig, A., Kleipool, Q., Bartstra, R., Landzaat, R., Leloux, J., Loots, E., Meijering, P., van der Plas, E., Rozemeijer, N., Vonk, F., Veefkind, P., 2020. In-flight calibration results of the TROPOMI payload on board the Sentinel-5 precursor satellite. Atmos. Meas. Tech. 13, 3561–3580. https://doi.org/10.5194/amt-13-3561-2020.
Lyapustin, A., Wang, Y., Laszlo, I., Kahn, R., Korkin, S., Remer, L., et al., 2011. Multiangle implementation of atmospheric correction (MAIAC): 2. Aerosol algorithm. Journal of Geophysical Research: Atmospheres 116 (D3), 3211. https://doi.org/10.1029/2010JD014986.
Lyapustin, Alexei, Wang, Y., Korkin, S., Huang, D., 2018. MODIS collection 6 MAIAC algorithm. Atmos. Meas. Tech. 11, 5741–5765. https://doi.org/10.5194/amt-11-5741-2018.
Maignan, F., Breon, F.M., Lacaze, R., 2004. Bidirectional reflectance of earth targets: evaluation of analytical models using a large set of spaceborne measurements with emphasis on the hot spot. Remote Sens. Environ. 90, 210–220.
Maignan, F., Bréon, F.M., Fédèle, E., Bouvier, M., 2009. Polarized reflectances of natural surfaces: Spaceborne measurements and analytical modeling. Remote Sens. Environ. 113 (12), 2642–2650. https://doi.org/10.1016/j.rse.2009.07.022.
Martin, R.V., 2008. Satellite remote sensing of surface air quality. Atmos. Environ. 42 (34), 7823–7843. https://doi.org/10.1016/J.ATMOSENV.2008.07.018.
Mishchenko, M.I., Travis, L.D., 1997. Satellite retrieval of aerosol properties over the ocean using measurements of reflected sunlight: effect of instrumental errors and aerosol absorption. J. Geophys. Res. Atmos. 102 (D12), 13543–13553. https://doi.org/10.1029/97JD01124.
Mishchenko, M.I., Travis, L.D., Lacis, A.A., 2002. Scattering, Absorption and Emission of Light by Small Particles. Cambridge University press.
Mischenko, M.I., Travis, L.D., 1997. Satellite retrieval of aerosol properties over the ocean using polarization as well as intensity of reflected light. J. Geophys. Res. 102, 16989–17013.
Mishchenko, M.I., Cairns, B., Hansen, J.E., Travis, L.D., Burg, R., Kaufman, Y.J., et al., 2004. Monitoring of aerosol forcing of climate from space: analysis of measurement requirements. J. Quant. Spectrosc. Radiat. Transf. 88, 149–161. https://doi.org/10.1016/j. jqsrt.2004.03.030.
Monahan, E.C., O'Muircheartaigh, L., 1980. Optimal power-law description of oceanic whitecap coverage dependence on wind speed. Journal of physical oceanography 10 (12), 2094–2099. https://doi.org/10.1175/1520-0485(1980)010<2094:OPLDOO>2.0.CO;2.
O'Neill, N.T., Eck, T.F., Smirnov, A., Holben, B.N., Thulasiraman, S., 2003. Spectral discrimination of coarse and fine mode optical depth. Journal of Geophysical Research D: Atmospheres 108 (17). https://doi.org/10.1029/2002jd002975.
Popp, T., de Leeuw, G., Bingen, C., Brühl, C., Capelle, V., Chedin, A., et al., 2016. Development, production and evaluation of aerosol climate data records from European satellite observations (Aerosol_cci). Remote Sens. (Basel) 8 (5), 421. https://doi.org/10.3390/rs8050421.
Reid, J.S., Koppmann, R., Eck, T., Eleuterio, D., 2005. A review of biomass burning emissions part II: intensive physical properties of biomass burning particles. Atmos. Chem. Phys. 5, 799–825.
Remer, L.A., Kaufman, Y.J., Tanre, D., Mattoo, S., Chu, D.A., Martins, J.V., et al., 2005. The MODIS aerosol algorithm, products, and validation. J. Atmos. Sci. 62, 947–973. https://doi.org/10.1175/JAS3385.1.
Ross, J., 1981. The Radiation Regime and Architecture of Plant Stands. The Radiation Regime and Architecture of Plant Stands. Dr W. Junk Publishers, The Hague, Netherlands.
Roujean, J.L., Leroy, M., Deschamps, P.Y., 1992. A bidirectional reflectance model of the Earth's surface for the correction of remote sensing data. J. Geophys. Res. Atmos. 97 (D18), 20455–20468. https://doi.org/10.1029/92JD01411.
Sayer, A.M., Hsu, N.C., Lee, J., Bettenhausen, C., Kim, W.v., Smirnov, A., 2018a. Satellite Ocean aerosol retrieval (SOAR) algorithm extension to S-NPP VIIRS as part of the "deep blue" aerosol project. J. Geophys. Res. Atmos. 123 (1), 380–400. https://doi.org/10.1002/2017JD027412.
Sayer, A.M., Hsu, N.C., Lee, J., Kim, W.V., Dubovik, O., Dutcher, S.T., et al., 2018b. Validation of SOAR VIIRS Over-Water Aerosol Retrievals and Context Within the Global Satellite Aerosol Data Record. Journal of Geophysical Research: Atmospheres 123 (23). https://doi.org/10.1029/2018JD029465, 2018JD029465.
Schaaf, C., Wang, Z., 2015a. MCD43C1 MODIS/Terra+Aqua BRDF/AlbedoModel Parameters Daily L3 Global 0.05Deg CMG V006 [Data set]. NASA EOSDIS Land Processes DAAC. Accessed 2020-09-14 from. https://doi.org/10.5067/MODIS/MCD43C1.006.
Schaaf, C., Wang, Z., 2015b. MCD43C3 MODIS/Terra+Aqua BRDF/Albedo Albedo Daily L3 Global 0.05Deg CMG V006 [Data set]. NASA EOSDIS Land Processes DAAC. Accessed 2020-09-14 from. https://doi.org/10.5067/MODIS/MCD43C3.006.
Schaaf, C.B., Gao, F., Strahler, A.H., Lucht, W., Li, X., Tsang, T., et al., 2002. First operational BRDF, albedo nadir reflectance products from MODIS. Remote Sens. Environ. 83 (1–2), 135–148. https://doi.org/10.1016/S0034-4257(02)00091-3.
Schutgens, N., Dubovik, O., Hasekamp, O., Torres, O., Jethva, H., Leonard, P.J., Litvinov, P., et al., 2021. AEROCOM and AEROSAT AAOD and SSA study – Part 1 : Evaluation and intercomparison of satellite measurements. Atmos. Chem. Phys 21 (9), 6895–6917. https://doi.org/10.5194/acp-21-6895-2021.
Sinyuk, A., Holben, B.N., Eck, T.F., Giles, D.M., Slutsker, I., Korkin, S., et al., 2020. The AERONET version 3 aerosol retrieval algorithm, associated uncertainties and comparisons to version 2. Atmos. Meas. Tech. 13 (6), 3375–3411. https://doi.org/10.5194/amt-13-3375-2020.
Strahler, A.H., Muller, J., Lucht, W., Schaaf, C., Tsang, T., Gao, F., et al., 1999. MODIS BRDF/albedo product: algorithm theoretical basis document version 5.0. MODIS Documentation 23 (4), 42–47.
Tanré, D., Bréon, F.M., Deuzé, J.L., Dubovik, O., Ducos, F., François, P., et al., 2011. Remote sensing of aerosols by using polarized, directional and spectral measurements within the A-train: the PARASOL mission. Atmos. Meas. Tech. 4 (7), 1383–1395. https://doi.org/10.5194/amt-4-1383-2011.
Thieuleux, F., Moulin, C., Breon, F.-M., Maignan, F., Poitou, J., Tanré, D., 2005. Remote sensing of aerosols over the oceans using MSG/SEVIRI imagery. Annales Geophysicae 23, 3561–3568. Copernicus GmbH.
Tilstra, L.G., Tuinder, O.N.E., Wang, P., Stammes, P., 2017. Surface reflectivity climatologies from UV to NIR determined fromEarth observations by GOME-2 and SCIAMACHY. J. Geophys. Res. 122 (7), 4084–4111. https://doi.org/10.1002/2016JD025940.
Tilstra, L.G., de Graaf, M., Wang, P., Stammes, P., 2020. In-orbit earth reflectance validation of TROPOMI on board the Sentinel-5 precursor satellite. Atmos. Meas. Tech. 13, 4479–4497. https://doi.org/10.5194/amt-13-4479-2020.
Tilstra, Lieuwe G., Tuinder, O.N.E., Wang, P., Stammes, P., 2021. Directionally dependent Lambertian-equivalent reflectivity (DLER) of the Earth's surface measured by the GOME-2 satellite instruments. Atmos. Meas. Tech. 14 (6), 4219–4238. https://doi.org/10.5194/amt-14-4219-2021.
Tilstra, L.G., de Graaf, M., Trees, V.J.H., Litvinov, P., Dubovik, O., Stammes, P., 2024. A directional surface reflectance climatology determined from TROPOMI observations. Atmos. Meas. Tech. 17, 2235–2256.
Torres, O., Tanskanen, A., Veihelmann, B., Ahn, C., Braak, R., Bhartia, P.K., et al., 2007. Aerosols and surface UV products from Ozone Monitoring Instrument observations: An overview. Journal of Geophysical Research 112 (D24), D24S47. https://doi.org/10.1029/2007JD008809.
Torres, O., Ahn, C., Chen, Z., 2013. Improvements to the OMI near-UV aerosol algorithm using A-train CALIOP and AIRS observations. Atmos. Meas. Tech. 6 (11), 3257. https://doi.org/10.5194/amt-6-3257-2013.
Travis, L.D., 1992. Remote sensing of aerosols with the earth observing scanning Polarimeter. Proc. SPIE 1747, 154–164. https://doi.org/10.1117/12.138823.
Travis, L.D., 1993. Earth observing system Polarimeter. In: Hansen, J., Rossow, W., Fung, I. (Eds.), Long-Term Monitoring of Global Climate Forcings and Feedbacks; NASA CP-3234. NASA, Washington, DC, pp. 40–46.
TROPOMI, 2022a. Product User Manual (PUM) GRASP BRDF + AOD: issue 1.0 date.
TROPOMI, 2022b. Final Report (FR): GRASP BRDF + AOD. Source: GRASP/KNMI; issue 1.0.
TROPOMI ATBD of the KNMI Aerosol Optical Thickness: KNMI AOT, 2022. Source: KNMI; issue 3.0.0.
TROPOMI ATBD: GRASP BRDF + AOD, 2021. Source: GRASP; issue 1.0.
TROPOMI L1B Specification, 2022. Input/output data specification for the TROPOMI L01b data processor. Source: KNMI; issue 11.0.0.
Tsang, L., Kong, J.A., Shin, R.T., 1985. Theory of microwave remote sensing. Wiley, NewYork.
Van de Hulst, H.C., 1957. Light Scattering by Small Particles. Wiley, New York. https://doi.org/10.1063/1.3060205. Chapman and Hall, London.
Veefkind, J.P., Aben, I., McMullan, K., Förster, H., de Vries, J., Otter, G., et al., 2012. TROPOMI on the ESA Sentinel-5 precursor: a GMES mission for global observations of the atmospheric composition for climate, air quality and ozone layer applications. Remote Sens. Environ. 120 (2012), 70–83. https://doi.org/10.1016/j.rse.2011.09.027.
Vermote, E.F., Kotchenova, S., 2008. Atmospheric correction for the monitoring of land surfaces. J. Geophys. Res. Atmos. 113 (D23), 23–90. https://doi.org/10.1029/2007JD009662.
Voss, K.J., Morel, A., Antoine, D., 1996. Detailed validation of the bidirectional effect in various case 1 waters for application to ocean color imagery. J. Geoph. Res. 14, 361–14,371, 101, No C6.
Wang, Z., Schaaf, C.B., Sun, Q., Shuai, Y., Román, M.O., 2018. Capturing rapid land surface dynamics with collection V006 MODIS BRDF/NBAR/albedo (MCD43) products. Remote Sens. Environ. 207, 50–64. https://doi.org/10.1016/J.RSE.2018.02.001.
Wanner, W., Li, X., Strahler, A.H., 1995. On the derivation of kernels for kernel-driven models of bidirectional reflectance. J. Geophys. Res. Atmos. 100 (D10), 21077–21089. https://doi.org/10.1029/95JD02371.
Washington, R., Todd, M.C., 2005. Atmospheric controls on mineral dust emission from the Bodélé depression, Chad: the role of the low level jet. Geophys. Res. Lett. 32 (17).